Discovery of 100 supernovae among $700,000$ Sloan spectra: the Type-Ia supernova rate versus galaxy mass and star-formation rate at redshift ~ 0.1

Or Graur[1,2][*] and Dan Maoz[1]

[1]*School of Physics and Astronomy, Tel-Aviv University, Tel-Aviv 69978, Israel*
[2]*Department of Astrophysics, American Museum of Natural History, Central Park West and 79th Street, New York, NY 10024-5192, USA*

4 September 2012

ABSTRACT
Using a method to discover and classify supernovae (SNe) in galaxy spectra, we find 90 Type Ia SNe (SNe Ia) and 10 Type IIP SNe among the $\sim 700,000$ galaxy spectra in the Sloan Digital Sky Survey Data Release 7 that have VESPA-derived star-formation histories (SFHs). We use the SN Ia sample to measure SN Ia rates per unit stellar mass. We confirm, at the median redshift of the sample, $z = 0.1$, the inverse dependence on galaxy mass of the SN Ia rate per unit mass, previously reported by Li et al. (2011b) for a local sample. We further confirm, following Kistler et al. (2011), that this relation can be explained by the combination of galaxy 'downsizing' and a power-law delay-time distribution (DTD; the distribution of times that elapse between a hypothetical burst of star formation and the subsequent SN Ia explosions) with an index of -1, inherent to the double-degenerate progenitor scenario. We use the method of Maoz et al. (2011) to recover the DTD by comparing the number of SNe Ia hosted by each galaxy in our sample with the VESPA-derived SFH of the stellar population within the spectral aperture. In this galaxy sample, which is dominated by old and massive galaxies, we recover a 'delayed' component to the DTD of $4.5 \pm 0.6 \times 10^{-14}$ SNe $M_\odot^{-1}$ yr^{-1} for delays in the range > 2.4 Gyr. The mass-normalized SN Ia rate, averaged over all masses and redshifts in our galaxy sample, is $R_{Ia,M}(z = 0.1) = 0.10 \pm 0.01$ SNuM, and the volumetric rate is $R_{Ia,V}(z = 0.1) = 0.25 \pm 0.03 \times 10^{-4}$ SNe yr^{-1} Mpc^{-3}. This is the most precise SN Ia rate measurement at this redshift, and is consistent with rates and the rate evolution from other SN Ia surveys.

Key words: methods: observational – surveys – supernovae: general

1 INTRODUCTION

The nature of the stellar system that ends up exploding as a type Ia supernova (SN Ia) is still uncertain (see Howell 2011 and Maoz & Mannucci 2011 for recent reviews). While the progenitor is most probably a carbon-oxygen white dwarf (CO WD; Nugent et al. 2011; Bloom et al. 2012), in order for it to explode it must be ignited. The current consensus is that the WD is in a binary system, through which it accretes mass until the pressure or the temperature in the WD core rise high enough to ignite carbon and initiate a thermonuclear runaway. The two leading scenarios for the nature of the progenitor system are the single degenerate scenario (SD; Whelan & Iben 1973) in which the WD accretes mass from a main-sequence, helium, or giant star,

while in the double degenerate scenario (DD; Iben & Tutukov 1984; Webbink 1984) the WD merges with a second CO WD through loss of energy and angular momentum to gravitational waves.

Theoretical and observational evidence exists both for, and against, each of the progenitor scenarios. The SD scenario, long held to be the more likely progenitor option, has been called into question by some recent observations. Pre-explosion images and early multi-wavelength data for SN2011fe have ruled out a red giant as the binary companion in that explosion (Li et al. 2011c; Chomiuk et al. 2012; Horesh et al. 2012; Brown et al. 2012). All possible SD companions, including main sequence stars, have been ruled out in the case of the SN Ia remnant SNR 0509-67.5 in the Large Magellanic Cloud (Schaefer & Pagnotta 2012, but see Di Stefano & Kilic 2012 and Shappee, Kochanek, & Stanek 2012). Sternberg et al. (2011) have made a statistical argument

[*] E-mail: orgraur@astro.tau.ac.il

that up to 25 per cent of SNe Ia in spiral galaxies may have sodium absorption lines in their spectra (see also Patat et al. 2007; Simon et al. 2009), the result of interaction with circumstellar material which could originate from a wind from a SD companion. Dilday et al. (2012) have found evidence of circumstellar material around the SN Ia PTF11kx, which they explain as the result of a symbiotic nova progenitor, similar to RS Ophiuchi. However, such events probably constitute only 0.1–1 per cent of all SNe Ia.

As for the DD scenario, Badenes & Maoz (2012) have recently measured the Galactic merger rate of WD–WD binary systems in the Sloan Digital Sky Survey (SDSS; York et al. 2000) and found it to be similar to the Galactic SN Ia rate (although only $\sim$ 10 per cent of the merger rate involves mergers above the Chandrasekhar mass). The DD scenario has long been disfavored by theoretical studies that predict that the merger of WDs of unequal mass would lead to an accretion-induced collapse to a neutron star, rather than to a SN Ia (Nomoto & Iben 1985; Shen et al. 2012; see, however, Pakmor et al. 2010, 2011, 2012; van Kerkwijk, Chang, & Justham 2010).

Some evidence favoring the DD scenario has emerged from reconstructions of the delay-time distribution (DTD; the distribution of times that elapse between a hypothetical δ-function-like burst of star formation and the subsequent SN Ia explosions). Different progenitor models predict different forms for the DTD (see Wang & Han 2012 for a recent review). A power-law DTD with an index of ~ -1 is inherent to the DD scenario, if the distribution of initial separations between the merging WDs is roughly a power law of that index (see, e.g., Maoz & Mannucci 2011). DTDs from SD models generally cut off after a few Gyr, although extended DTDs in the SD context have been predicted as well (e.g., Di Stefano, Voss, & Claeys 2011; Hachisu, Kato, & Nomoto 2012).

Recent studies, using various SN samples, environments, and redshift ranges, have consistently measured a power-law DTD of the form t^{-1} (see Maoz & Mannucci 2011 for a review). A measurement of the SN Ia rates in elliptical galaxies as a function of luminosity-weighted galaxy age by Totani et al. (2008) was best-fitted by a power-law DTD of the approximate t^{-1} form. Galaxy clusters, where most of the star formation is thought to have occurred in one burst at $z \approx 3$, have also yielded SN Ia rates consistent with such a power-law DTD (Sharon et al. 2010; Maoz, Sharon, & Gal-Yam 2010; Barbary et al. 2012b; Sand et al. 2012). Measurements of the volumetric rate of SNe Ia in field galaxies as a function of the cosmic star formation history (SFH) point to a t^{-1} DTD [see Graur et al. 2011 for a compilation of such surveys and their results up to 2011, and Perrett et al. 2012 (P12) for subsequent surveys out to $z \approx 1$].

The dependence of SN Ia rates on host-galaxy mass and star-formation rate provides a further probe of the DTD. Mannucci et al. (2005) and Mannucci, Della Valle, & Panagia (2006) showed that a broad distribution of delay times is required in order to explain the increase in the SN Ia rate per unit stellar mass in bluer galaxies, with a t^{-1} DTD providing an excellent fit (see Maoz & Mannucci 2011). Li et al. (2011b, L11) measured SN Ia rates per unit stellar mass in the local Universe and found that they followed a 'rate-size' relation, whereby less-massive galaxies have higher mass-normalized SN Ia rates than more massive galaxies. Kistler et al. (2011)

showed that the rate-size relation could be explained by the combination of galaxy 'downsizing' (i.e., older galaxies tend to be more massive than younger galaxies) and a power-law DTD of index -1.

Brandt et al. (2010) and Maoz et al. (2011, M11) introduced a method for recovering the DTD while accounting for the detailed SFHs of the individual monitored galaxies. M11 used this method on a subsample of the Lick Observatory SN Search sample (LOSS; Leaman et al. 2011; Li et al. 2011a; L11), from which they recovered a DTD with both 'prompt' ($t < 420$ Myr) and 'delayed' ($t > 2.4$ Gyr) components. In Maoz, Mannucci, & Brandt (2012, M12), this method was applied to the SDSS-II sample of SNe (Dilday et al. 2010; Sako et al. 2011), from which a similar DTD with prompt, delayed, and 'intermediate' ($0.42 < t < 2.4$ Gyr) components was recovered, consistent with the t^{-1} form of previous studies.

Most SN surveys have been based on imaging, whether by monitoring specific galaxy samples, or volumes of space and the galaxies that they include. However, it is also possible to discover SNe serendipitously among large samples of galaxy spectra, in which the galaxy region covered by the spectral aperture happens to host a SN during the time of exposure. Advantages of such samples are that the spectra, and hence classification, of transients is immediately available. Furthermore, the availability of the spectra of the stellar populations in the specific galactic regions that were effectively 'monitored' permits deriving accurate rates and DTDs.

In this paper, we discover a new SN sample by searching for, and classifying, transients (including, but not limited to, SNe Ia) among $\sim$ 700,000 galaxy spectra from the 7th data release of the SDSS (SDSS DR7; Abazajian et al. 2009). Madgwick et al. (2003, M03) were the first to discover SNe Ia in SDSS galaxy spectra (in SDSS DR1). They found 19 SNe Ia among $\sim$ 100,000 galaxy spectra, from which they estimated the SN Ia rate at $z \approx 0.1$. Krughoff et al. (2011, K11) made a similar measurement, using the larger galaxy sample in SDSS DR5, finding 52 SNe Ia among $\sim$ 350,000 galaxies. As detailed below, in this paper we analyse a larger sample, using a number of improvements in transient detection, classification, and rate analysis. We provide the details of our galaxy sample in Section 2. In Section 3 we describe our discovery and classification routine and assess its efficiency and purity. In Section 4 we present our SN sample. Using our SN Ia sample, in Section 5 we measure mass-normalized SN Ia rates, convert them to a volumetric rate, and compare them to previous results. In this section we also recover the delayed component of the DTD using the direct recovery method of M11. We summarize and discuss our results in Section 6.

Throughout this paper we assume a Λ-cold-dark-matter cosmological model with parameters $\Omega_\Lambda = 0.7$, $\Omega_m = 0.3$, and $H_0 = 70$ km s^{-1} Mpc^{-1}. Magnitudes are on the AB system (Oke & Gunn 1983), unless noted otherwise.

2   GALAXY SAMPLE

For the purpose of this work we used the 776,447 galaxy spectra in SDSS DR7 which have SFHs obtained by Tojeiro et al. (2009, T09) using the VErsatile SPectral Analysis code

(VESPA[1]; Tojeiro et al. 2007). As in M11 and M12, we use the total formed stellar masses fit by VESPA to the SDSS spectra in three time bins: 0–0.42 Gyr, 0.42–2.4 Gyr, and > 2.4 Gyr (corresponding to bins $24 + 25$, 26, and 27 in T09). We specifically use the VESPA reconstruction that assumes a single dust component and utilises the Maraston (2005) spectral synthesis models. A Chabrier (2003) stellar initial mass function is assumed in T09, and this assumption therefore propagates into the mass normalization of the SN Ia rates we report. T09 measured the total mass in the SDSS fiber aperture and then applied an aperture correction to obtain the total mass in the entire galaxy (see their equation 22). Since, for rate purposes, we are interested in the stellar mass inside the fiber aperture (which was the stellar mass that was effectively monitored for SNe), we reverse this aperture correction, and propagate the uncertainties accordingly. We reduce the masses in each time bin by a further factor of 0.55, due to the different flux calibrations between SDSS DR5 and DR7 (R. Tojeiro, private communication, see M12 for a detailed discussion). Of the 776,447 galaxies in our sample, 52,016 galaxies, constituting 6.7 per cent of the sample, have VESPA-derived masses only in a coarse bin in the time range > 0.42 Gyr (i.e., in bin 29). This precludes using these galaxies, as we cannot know how to distribute these masses between the 0.42–2.4 Gyr and > 2.4 Gyr bins. Furthermore, we exclude those galaxies for which the VESPA SFH has a reduced χ^2 value in the range $\chi^2 > 10$, are at redshift $z > 1$, or that have less than 500 good pixels in their spectra, according to the MASK array included by SDSS for each spectrum [we use only those pixels that have a '0' (good) or '40000000' (emission line) bit flag]. These cuts reduce our sample to 707,792 galaxies.

Of the galaxies in the sample, 29,066 galaxies have more than one spectrum, observed on different dates. Of these galaxies, after applying the above cuts, we consider in our rates analysis only the spectra that are spaced at least 60 days apart, in order to assure independent search epochs. Five of the host galaxies of the SNe Ia that we present below have multiple observations (namely, 0394-51812-554, 0418-51884-144, 1298-52964-304, 1782-53383-517, and 2019-53430-010). Throughout this work we refer to SNe discovered in SDSS spectra according to the plate, modified Julian date (MJD), and fiber in which they are discovered (e.g., 0814-52443-249 was observed on MJD 52443, or June 18 2002, in the galaxy targeted by the 249th fiber of plate 814, where each SDSS plate contains 640 fibers). The above cut leaves 26,592 multiply-observed galaxies: 12,991 with two observations; 197 with three epochs; 11 with four; three with five; and two galaxies with six epochs.

We classify the galaxies in our sample according to their specific star-formation rate (sSFR), which is computed as the VESPA mass formed in bins 24+25, divided by 420 Myr, and divided by the total formed mass. Following Sullivan et al. (2006b), we separate the galaxies into highly star-forming [$\log(\mathrm{sSFR/yr^{-1}}) \geqslant -9.5$], star-forming [$-12 \leqslant \log(\mathrm{sSFR/yr^{-1}}) < -9.5$], and passive [$\log(\mathrm{sSFR/yr^{-1}}) < -12$] galaxies. As we show in the upper panel of Fig. 1, our galaxy sample is dominated by massive, old galaxies, and consists of 54.5, 44.7, and 0.8 per
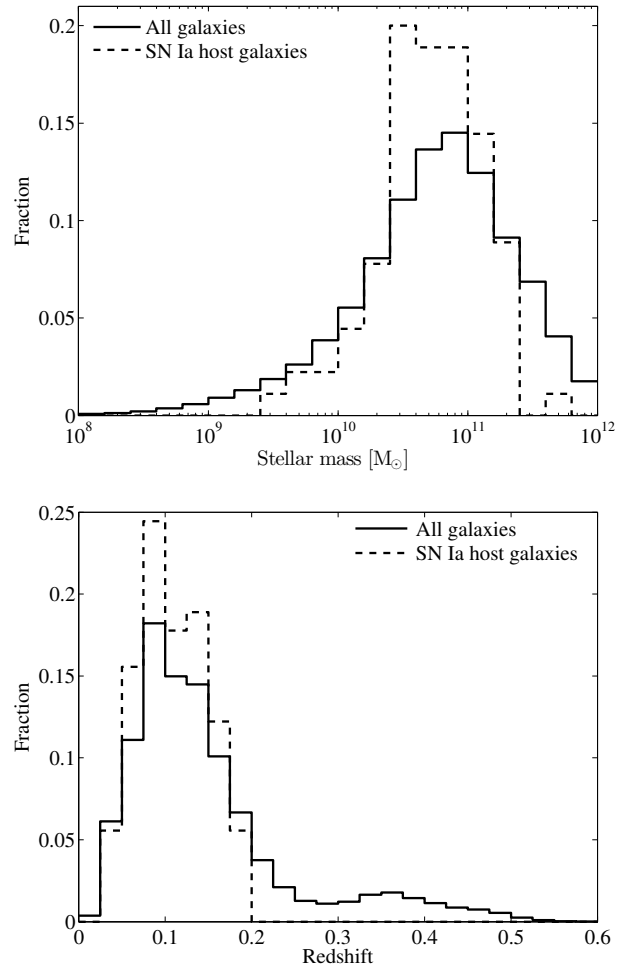
Figure 1. Total stellar mass (upper panel) and redshift (lower panel) distributions for all galaxies in our sample (solid curve) and SN Ia host galaxies (dashed curve).

cent passive, star-forming, and highly star-forming galaxies, respectively. The SN Ia host galaxy sample is similarly divided into 47.8, 52.2, and 0 per cent passive, star-forming, and highly star-forming galaxies, respectively. Since only 0.8 per cent of our galaxies are highly star-forming, we combine the star-forming and highly star-forming galaxies into one category, which we label 'star-forming galaxies' (i.e., with $\log(\mathrm{sSFR/yr^{-1}}) \geqslant -12$). The lower panel of Fig. 1 shows the redshift distribution of our galaxy sample and SN Ia host-galaxy sample. The median redshifts of the galaxy and SN Ia host galaxy samples are $z = 0.11$ and $z = 0.09$, respectively. Due to the limits of our detection and classification process, we do not find SNe Ia above $z \approx 0.2$.

3 SUPERNOVA DISCOVERY AND CLASSIFICATION

3.1 Method

The galaxy spectra are first de-reddened according to Cardelli, Clayton, & Mathis (1989) and the $E(B - V)$ val-

---

[1] http://www-wfau.roe.ac.uk/vespa/

Table 1. Transient classification criteria

| Transient	SVD	SNID	SNID%
Ia	Ia	Ia	Ia$\geqslant 0.5$
Ia/Ic	Ia Ib/c	Ia or Ib/c	Ia$\geqslant 0.5$
Ib/c	Ib/c	Ib/c	Ib/c$\geqslant 0.5$
Ic/Ia	Ia or Ib/c	Ia or Ib/c	Ia< 0.5
IIb	Ib/c or IIb	Ib/c or IIb	Ib/c$\geqslant 0.5$
II	IIP, IIL, or IIn	IIP, IIL, or IIn	II$\geqslant 0.5$
LBV	LBV	LBV	
AGN[a]	AGN or other	AGN or other	

Note – In order to be classified into one of the SN subtypes in column 1, a candidate must meet both the SVD and SNID criteria in columns 2 and 3, and the fraction of best-fitting SNID templates in column 4. For example, if a candidate is fit as a SN IIP in the SVD stage, and as a SN IIL by SNID, and the fraction of best-fitting SNID templates is $\geqslant 0.5$, that candidate would be classified as a SN II. Otherwise, it would be discarded.

[a]AGNs were not required to be classified as such by both the SVD and SNID stages.

ues listed in the SDSS spectrum headers. The spectra are then masked according to the MASK array included for each spectrum.

In order to identify SNe in the SDSS DR7 galaxy spectra, we first subtract a model of the galaxy constructed from ten SDSS DR2 galaxy eigenspectra (Yip et al. 2004a), using singular value decomposition (SVD). At this stage, we discard spectra with best-fitting galaxy models with reduced $\chi_r^2 \leqslant 1$, as these spectra either do not host a transient, or have a too low signal-to-noise ratio (S/N). The residual spectrum obtained by subtracting the galaxy model is fit with a straight line in f_λ vs. wavelength, which is then subtracted. This 'flattened' residual is searched for 'features' by counting the number of continuous pixels above (or below) zero. The residual spectrum must have at least ten features, each $\geqslant 30$ pixels wide. These values were found to be optimal for discovering faint SNe, while reducing the number of false positives.

Every galaxy spectrum that satisfies the above criteria is then re-analysed by adding SN templates to the SVD-constructed galaxy model. We use the spectral library from the Supernova Identification code (SNID[2]; Blondin & Tonry 2007), which contains SN (Ia and core collapse), active galactic nucleus (AGN), luminous blue variable (LBV), flaring M dwarf, and galaxy spectra. For each SVD fit we compute a figure of merit, χ_λ^2, composed of the reduced χ^2 value, divided by the wavelength range covered by the specific transient template. This is necessary, as some transient templates cover small wavelength ranges due to the instrumental setups with which they were taken. Such templates would receive a low χ^2 value if they fit specific features in the residual spectrum, even though a different template from the same transient class that covers a larger wavelength range may not fit the rest of the residual. This can lead to the misclassification of transients (e.g., SNe Ia as core-collapse SNe). To overcome this problem, we keep only those transient templates in the SNID library that cover a wavelength range of at least 2,900 Å, reducing the SNID spectral library from 349 objects with 3,056 spectra to 304 objects with 2,952 spectra.
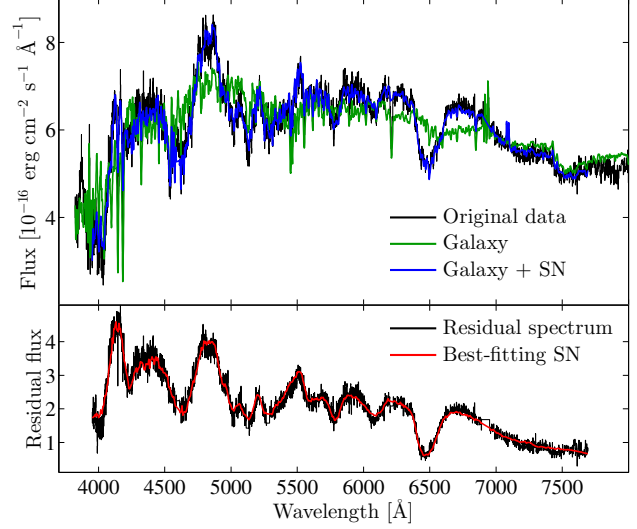
Figure 2. A SN Ia discovered in the SDSS galaxy spectrum 0424-51893-355 (plate-MJD-fiber) at $z = 0.054$. Top: the original galaxy spectrum (black) is fit with a galaxy model (green) composed of ten eigenspectra, resulting in a reduced $\chi_r^2 = 7.6$. When fit with both eigenspectra and transient templates (blue), a SN Ia template produces a reduced $\chi_r^2 = 1.1$. Bottom: residual spectrum (black) produced by subtracting the galaxy model from the original data. The best-fitting SN Ia template is shown in red.

Only transient models with a reduced χ_r^2 value smaller than the original-galaxy-fit χ_r^2 are considered for further analysis.

The residual spectrum with the best minimal χ_λ^2 is input to SNID for a second, independent classification, where the following criteria must be met:

(i) The residual must fit more than one template. This eliminates a large number of low-S/N false positives.
(ii) The best-fitting template must have rlap$\geqslant 5$, and lap$\geqslant 0.4$. The 'lap' parameter quantifies the amount of overlap between the residual spectrum and the transient templates at the correlation redshift, while 'rlap' is a quality parameter, where higher values denote better correlations (see Blondin & Tonry 2007 for a full description).
(iii) The best-fitting templates must be at a redshift within $\Delta z = 0.015$ of the SDSS-measured redshift.

A large number of false positives are culled at this stage, as some residual spectra with low S/N ratios might be fit with transient templates using SVD, but will be disqualified by SNID.

Finally, the candidate is classified into eight transient categories, according to the SVD and SNID best-fitting templates, and according to the percentage of SNID templates belonging to a specific category, which we call SNID%. The transient candidates are classified as Ia, Ib/c, IIb, II, LBV, or AGN. We also include two additional categories: Ia/Ic (Ic/Ia), which include SNe Ia (Ic) that were misclassified as SNe Ic (Ia). Were Ia/Ic SNe to be added to the SN Ia sample, they would carry a systematic uncertainty (e.g., if two SNe Ia/Ic are discovered, they would add a -2 systematic error to the number of SNe Ia). However, as detailed in

Table 2. SN Ia population fractions and luminosity functions

SN Ia subtype	fraction	adopted LF [Vega mag]
normal Ia	0.761	-19.42 ± 0.51
Ia-91bg	0.024	-18.30 ± 0.52
Ia-91T[a]	0.197	-19.90 ± 0.53
Ia-02cx[b]	0.018	
IIP	0.394	-16.41 ± 1.23
IIL	0.275	-18.19 ± 0.64
IIn	0.230	-17.61 ± 1.61
IIb	0.101	-17.40 ± 1.30
Ib	0.324	-17.76 ± 0.41
Ic	0.528	-16.79 ± 1.28
peculiar Ib/c	0.148	-16.25 ± 1.21

[a] This category includes SN2000cx and SN2006gz.
[b] As SN2002cx and SN2005hk were both as faint as SN-91bg-like SNe Ia, they were given its LF.

Table 3. Classification purity

		Planted as:		
		Ia	Ib/c	II
Classified as:	Ia	99.13	1.4	0.10
	Ia/Ic	0.68	5.6	0.24
	Ib/c	0.09	91.7	0.51
	Ic/Ia	0.08	1.2	0.11
	II	0.02	0.1	99.04

Note – All values are percentages.

Section 4, we find no such SNe. The classification rules are summarized in Table 1.

Along with the SNe in our sample, we also find ~ 980 AGNs. In order to check whether any of these AGN-hosting galaxies also host other types of transients, we re-analyse them one more time, using a combination of the galaxy eigenspectra, the Vanden Berk et al. (2001) composite AGN template (which is also included in the SNID spectral library), and all other transients in the SNID spectral library. In other words, whereas in the previous stage the data was fit with either an AGN or a different transient template, in this stage it is fit with both simultaneously. We find no other transients in these galaxies.

We do not mask galaxy emission lines in the first stage of analysis, as we have found that the emission lines have a negligible effect on our discovery success rate. However, since the strength of individual emission lines changes from galaxy to galaxy, they are not perfectly fit by the eigenspectra, contaminating the residual spectrum and causing SNID to misclassify SN candidates. In the re-analysis stage, we therefore mask the emission lines of Hα, Hβ, [OI] $\lambda 6300$, [OII] $\lambda 3727$, [OIII] $\lambda 4363, 4959, 5007$, NII $\lambda 6548, 6583$, and the Na D $\lambda 5890, 5896$ absorption feature. In Fig. 2 we show an example of a SN Ia discovered by our methodology.

3.2 Comparison with previous spectral supernova searches

As in this work, M03 and K11 used galaxy eigenspectra, obtained through principal component analysis, to subtract a galaxy model from the data. The residual spectrum, however, was analysed differently. M03 performed a wavelet transform on the residual to separate the SN signal from the noise. This resulted in a 'noiseless' signal which they compared, through cross-correlation, to a small set of SN Ia spectral templates. Such manipulation of the data carries the risk of introducing artificial features, and indeed we believe that some of the SNe reported by M03 may have been false detections (see below). K11 used the same Yip et al. (2004a) eigenspectra as in this work, together with an AGN template composed of the first two QSO eigenspectra from Yip et al. (2004b), and the Nugent, Kim, & Perlmutter (2002) SN Ia template. Their comparison to SN templates was done solely through SVD.

Our method differs in four main ways:

(i) We use the SNID as well as the SVD-derived χ^2 criterion. This allows us to cull false SN Ia candidates (as detailed in Section 3.1) and other false positives.

(ii) We have found that using an AGN template together with the galaxy eigenspectra 'robs' some of the continuum from a transient in the galaxy spectrum, making it harder to discover fainter SNe. Instead, as detailed in Section 3.1, we first find ~ 980 AGN-hosting galaxies, and search them for additional transients. By limiting the combination of the AGN template and the galaxy eigenspectra to these AGN-hosting galaxies alone, we assure that the AGN template does not affect the shape of the residual spectra in non-AGN-hosting galaxies.

(iii) By using SNID, and the SNID templates in the SVD phase, we can discover other types of transients, from core-collapse SNe to LBVs. Furthermore, SNID and the SVD phase are modular: new spectra can be added as they become available (e.g., for new types of transients, such as the super-luminous SNe).

(iv) The data are not manipulated in any way (e.g., there is no binning).

We recover all of the eight examples reported by K11 out of the 52 SNe Ia they discovered, except 0472-51955-247 (see their figure 8) which is hosted by a galaxy that is not included in our galaxy sample. Of the 19 SNe Ia reported in M03, we recover ten. Two of the 19 SNe are hosted by galaxies that are not included in our galaxy sample, as they do not have associated VESPA SFHs. Of the remaining seven SNe Ia, the residual spectra of the four galaxies hosting SN2000ga, SN2001ki, SN2001kl, and SN2001kr have no discernible SN Ia features, and we deem them false detections. SN2001kn and SN2001ks may be real SNe Ia, but were not detected by our methodology due to the low S/N of their residual spectra. Finally, SN2001kq is detected with a redshift that is higher by $\Delta z > 0.015$ than that of its host galaxy, and so is rejected by our detection and classification process. The redshift difference appears to be due to a rather poor best fit to a noisy residual spectrum, indicating a peculiar SN Ia. Differences in the SN Ia rate analysis between this work and M03 and K11 are discussed in Section 5.3.

3.3 Detection and classification efficiency

SNe may be missed by our discovery and classification process for numerous reasons, including poor data (such as spectra with large masked areas), low S/N, low contrast relative to the galaxy light, or failure to meet our classification criteria. In order to quantify these and other systematic effects, we simulate the discovery and classification efficiency of our
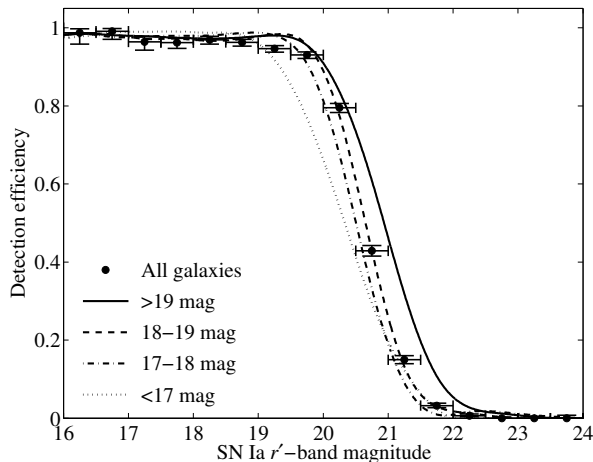
Figure 3. SN Ia detection efficiency as a function of SN Ia r'-band magnitude. Filled circles denote the fraction of fake SNe Ia discovered in all galaxies in 0.5-mag-wide bins. Error bars indicate 1σ binomial uncertainties. Curves are cubic spline fits to the detection-efficiency measurements of SNe Ia in host galaxies with r'-band magnitudes in different ranges, as marked.
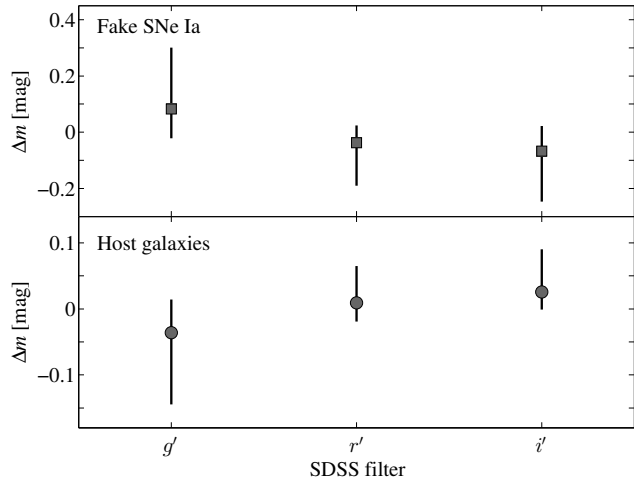

Figure 4. Distributions of differences between the planted and measured g'-, r'-, and i'-band magnitudes of the fake SNe Ia (filled squares) and their host galaxies (filled circles), respectively. The markers denote the medians of the distributions, and the vertical error bars denote the 16th and 84th percentiles.

method by planting fake SN spectra in a random selection of real galaxy spectra.

The fake SN spectra are drawn from the the subsample of SNID spectra spanning $\geqslant 2,900$ Å. In order to simulate the real distribution of SNe Ia in our sample, the host galaxies are chosen according to their sSFR. As the rate of SNe Ia is higher in more luminous galaxies, we favor in our simulation the selection of host galaxies based on luminosity, according to the dependence of the rate of SNe Ia on host-galaxy r'-band luminosity in figure 12 of Yasuda & Fukugita (2010). Furthermore, as the SN Ia rate in passive galaxies is $\sim 1/3$ the rate in star-forming galaxies (see figure 6 in Sullivan et al. 2006b), 25 (75) per cent of the host galaxies in the fake sample are chosen to be passive (star-forming) galaxies. Next, the SN Ia spectra are planted according to the luminosity functions (LFs) and subtype populations from Li et al. (2011a). The Li et al. (2011a) normal-Ia LF is centred on -18.67 mag (Vega), with a standard deviation of 0.51 mag. This LF is fainter than most measured SN Ia LFs, so we use instead the Yasuda & Fukugita (2010) value of -19.42 mag (Vega). We use the difference between these values (0.75 mag) to similarly brighten the mean values of the Li et al. (2011a) SN-subtype LFs. Table 2 lists the population fractions and adopted LFs we use for each SN subtype. Varying the mean brightness of the LFs (e.g., using the original Li et al. 2011a values) does not affect the overall shape of the resulting detection efficiency function.

For each fake spectrum we choose a random peak B-band magnitude from the appropriate LF, and translate it into a stretch value, s, according to the Perlmutter et al. (1999) stretch-luminosity relation

$$m_{B,s} = m_{B,1} + \alpha(s - 1), \qquad (1)$$

where $m_{B,s}$ is the peak B-band magnitude of the stretched light curve, $m_{B,1}$ is the peak B-band magnitude of a normal $s = 1$ SN Ia, and $\alpha = 1.52$ (Astier et al. 2006). From this

stretched light curve we choose a random epoch, and assign the fake spectrum the r'-band magnitude on that epoch. Following Sullivan et al. (2006a), we limit the stretch range to $0.6 < s < 1.4$.

We conduct three separate simulations, in each of which $\sim 10,000$ fake spectra of a specific SN subtype are planted in $\sim 75,000$ random galaxy spectra. The SN Ia simulation includes all normal SNe Ia, SN-91T-like SNe [including SN2000cx (Li et al. 2001) and SN2006gz (Hicken et al. 2007)], SN-91bg-like SNe, and SN2002cx-like SNe [i.e., SN2002cx (Li et al. 2003) and SN2005hk (Phillips et al. 2007)]. We do not include the peculiar SNe SN2002ic (Hamuy et al. 2003), SN2003fg (Howell et al. 2006), and SN2005gj (Prieto et al. 2007). The SN Ib/c simulation includes normal SNe Ib, SNe Ic, and SNe IIb, along with peculiar SNe Ib and broad-lined SNe Ic. The SN II simulation includes all SN IIP, SN IIL, and SN IIn spectra included in SNID.

Similarly to the SNe Ia, the SN Ib/c and SN II fakes are planted according to the LFs and population fractions presented in tables 6 and 7 of Li et al. (2011a). We apply the same magnitude correction of 0.75 mag to these LFs, which are presented in Table 2. Contrary to the fake SNe Ia, the fake SNe Ib/c and SNe II are only planted in star-forming galaxies, i.e., those galaxies with $\log(\text{sSFR/yr}^{-1}) \geqslant -12$.

Table 3 lists the purity of our classification method, i.e., what fraction of fake SNe were classified into the different subtypes listed in Table 1. The table shows that our code is efficient at classifying SNe Ia and SNe II. SNe Ib/c, however, are harder to classify, as they may appear similar to SNe Ia (especially SNe Ic that exhibit no hydrogen or helium in their spectra). There is a 1.4-per-cent chance that one of our SNe Ia is in fact a misclassified SN Ib/c. We take this into account by adding a systematic uncertainty of -1 to our sample of 90 SNe Ia, described in Section 4. Furthermore, there is a 5.6-per-cent probability that a SN Ib/c will be
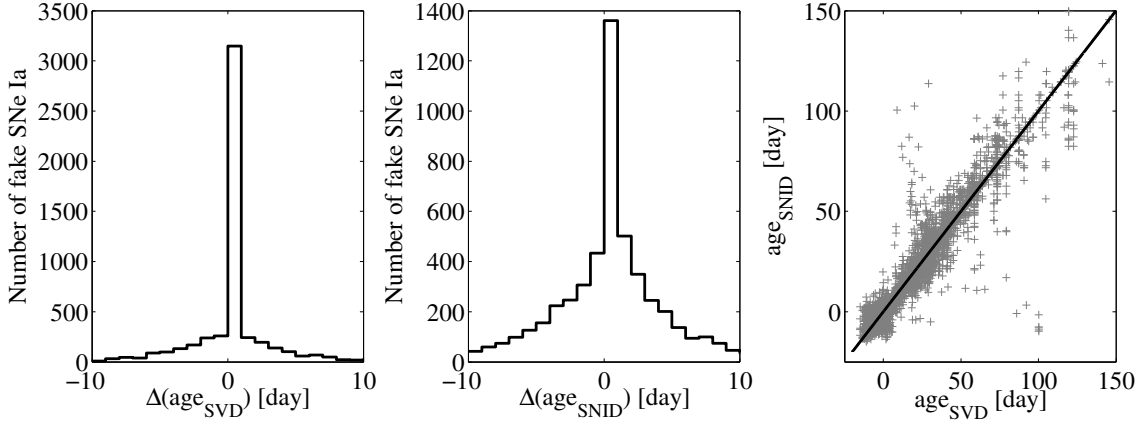
Figure 5. Left and centre: distributions of differences between the planted and recovered SVD- and SNID-derived ages of the fake SNe Ia, respectively, in 1-day-sized bins. Right: comparison of the SVD- and SNID-derived ages (crosses). The solid curve represents the 1:1 line.

misclassified as a Ia/Ic. However, we have no such SNe in our SN Ia sample.

We present the results of our SN Ia simulation in Figures 3–5. Fig. 3 shows our SN Ia detection efficiency as a function of the r'-band apparent magnitude of the planted SNe. We reach 50 per cent efficiency at $r' = 20.7$ mag. Since the brightness of the host galaxy affects the probability of detecting the SN (i.e., it is easier to discover SNe in fainter galaxies, and vice versa), we divide the SN Ia detection efficiency measurements shown in Fig. 3 into four subsets, according to the host-galaxy r'-band magnitudes. These subsets are: $r'_h > 19, 18 < r'_h \leqslant 19, 17 < r'_h \leqslant 18$, and $r'_h \leqslant 17$ mag. To the efficiency curves of each of these subsets we fit a cubic spline.

In Fig. 4 we show the distributions of the differences between the planted and recovered apparent magnitudes, Δm, of the fake SNe Ia, and their host galaxies, in the g', r', and i' bands. Because the transient spectra are not orthogonal with the set of galaxy eigenspectra, there is a flow of flux between them, which causes the SNe to appear brighter, on average, in the g' band, and fainter in the r' and i' bands. The host galaxies, conversely, appear fainter and brighter, respectively, in these bands, as shown. Throughout this paper we report SN and host-galaxy apparent magnitudes in the r' band, where the dispersion in Δm is smallest. Moreover, as the average offset in the measured r'-band magnitude of the SNe Ia caused by the flux flow is negligible, and as the uncertainties in brightness are smaller than the 0.5-mag-wide bins we use for the detection efficiency measurements of Fig. 3, we do not consider this offset any further.

The left and centre panels of Fig. 5 show the distributions of differences between the planted and SVD- and SNID-derived ages, respectively, in 1-day-sized bins. The right panel of Fig. 5 shows a comparison of the SVD- and SNID-derived ages. While the derived ages are almost always within ± 1 day of the planted values, the comparison between the SVD- and SNID-derived ages in the right panel of Fig. 5 shows that there is a larger source of systematic uncertainty contributing to the discrepancy between them. If we assume that the overall uncertainty is identical for all the SNe Ia, then we can estimate it by fitting the SVD-

to the SNID-derived ages and setting $\chi^2 = 1$. After limiting the ages of the fake SNe Ia to the range of the real SNe Ia in our sample, -10–55 days relative to B-band maximum light, we estimate the overall uncertainty in the age of the SNe Ia to be ± 6 days. In a similar manner, we estimate the uncertainty in the ages of the SNe IIP to be ± 33 days.

3.4 Supernova age and stretch recovery efficiency

In order to measure the stretches of the SNe Ia in our sample, we substitute the SNID templates used in the discovery phase with the Guy et al. (2007) SALT2[3] templates. Similarly to the Yip et al. (2004a) eigenspectra, the SALT2 templates are composed of two base spectral sequences: $M_0(p, \lambda)$ and $M_1(p, \lambda)$, where p is time since maximum light in the rest-frame B-band, λ is the rest-frame wavelength, $M_0(p, \lambda)$ is the average time sequence of eigenspectra, and $M_1(p, \lambda)$ is the spectral sequence of variations induced by the stretch of the SNe. Following equation 1 in Guy et al. (2007), we add the SALT2 eigenspectra linearly:

$$F(p, \lambda) = x_0 \times [M_0(p, \lambda) + x_1 M_1(p, \lambda)], \qquad (2)$$

but without the exponential colour correction. The variable x_1 can be converted into the stretch parameter s by using the Guy et al. (2007) transformation

$$s = 0.98 + 0.091 x_1 + 0.003 x_1^2 - 0.00075 x_1^3. \qquad (3)$$

We first gauge the accuracy of our stretch measurements by planting fake SNe Ia made up of the SALT2 templates with predetermined stretches. Fig. 6 shows the distribution of differences between the planted and recovered stretch values for a sample of 7,200 fake SNe Ia planted using the SALT2 templates, in bins of $\Delta s = 0.1$. The distribution is more sharply peaked than a Gaussian, and the range of stretches enclosing 68 per cent of the area is ± 0.03. We take this to be the uncertainty of our stretch measurements. As in Section 3.3, fitting the SALT2-derived ages to those derived by SVD results in the same uncertainty of ± 6 days.

---

[3] http://supernovae.in2p3.fr/~guy/salt/
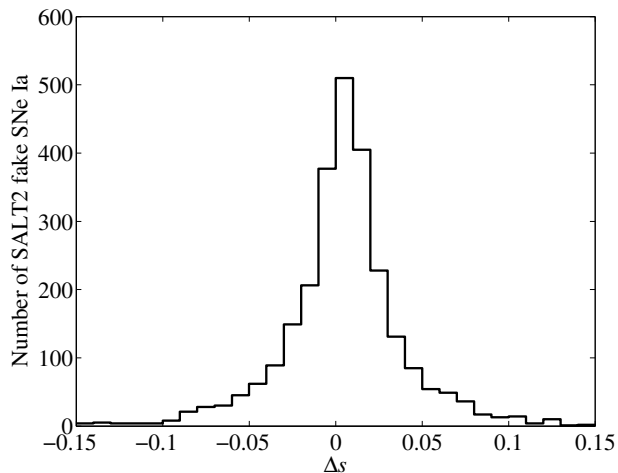
**Figure 6.** Results of using our discovery code with the SALT2 templates: the distribution of differences between the planted and recovered stretch values for a sample of 7,200 fake SNe Ia planted using the SALT2 templates.

4   SUPERNOVA SAMPLE

We find a total of 100 SNe, of which 90 are SNe Ia and 10 are SNe IIP. Table 4 lists the SNe and their properties. The residual spectra and best-fitting SN templates are shown in Figures 8 and 9. Each SN is listed according to the plate, MJD, and fiber in which it was discovered. We measure the r'-band magnitudes of the SNe by performing synthetic photometry on the SN residual spectrum, as obtained by subtracting the galaxy model from the original data. Similarly, the r'-band magnitudes of the SN host galaxies are measured using synthetic photometry on the original data, after subtracting the SN residual. Finally, we measure the stretch of each SN using the SALT2 templates, as detailed in Section 3.4.

Apart from these SNe, we detect $\sim$ 980 AGNs and several dozen transients which might be either SNe IIn or AGNs. Some SN IIn spectra, which exhibit broad hydrogen lines, are indistinguishable, without further spectroscopic or photometric followup, from AGNs, which have similar emission lines.

Some of the SNe Ia in our sample are sufficiently bright so as to significantly distort the shape of the combined galaxy+SN spectrum. This results in a systematically biased VESPA fit and an incorrect SFH for the host galaxy. In order to correct this, we replace the SFHs of such host galaxies with those of 'surrogate' galaxies that did not host SNe, by fitting the continuum of the SN host galaxy with those of all galaxies within our galaxy sample that have the same redshift, within $\Delta z = 5 \times 10^{-4}$, and r'-band magnitude within $\Delta m = 0.05$ mag. We inspect by eye the resulting five best-fitting galaxies. In most cases, we select the galaxy with the minimal reduced χ_r^2 value as the surrogate galaxy. In some cases, a better fit, with a χ_r^2 value that is slightly larger (up to two tenths) of the minimal χ_r^2, is discernible by eye, and we choose it instead. We find that no surrogates are necessary for host galaxies where the contrast between the host and the SN Ia is $\leqslant 0.1$. For SN-hosting galaxies with multiple, SN-free observations (i.e., 0394-51812-554, 0418-
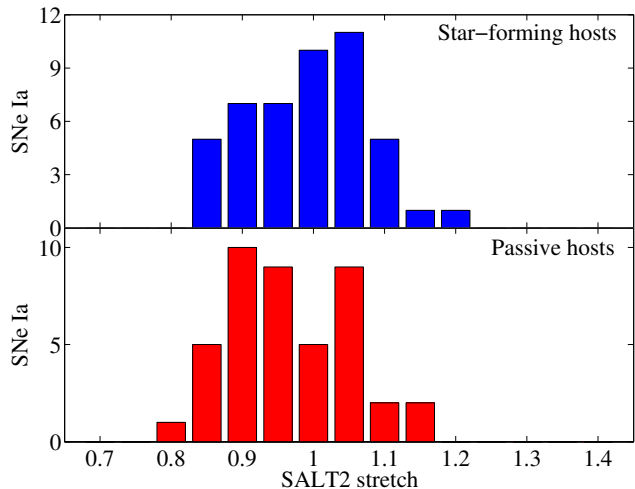
Figure 7. Stretch values for 90 SNe Ia, as measured using the SALT2 templates. The stretch values in the upper (lower) panel are for the 47 (43) SNe Ia in star-forming (passive) galaxies, where star-forming (passive) galaxies are chosen to have $\log(\mathrm{sSFR/yr}^{-1})$ above (below) -12.

51884-144, 1298-52964-304, and 2019-53430-010), we use the formed masses derived from the VESPA fits to the SN-free galaxy spectra.

Figure 7 shows the stretch distributions of the 90 SNe Ia in our sample. Many previous studies have found that star-forming galaxies tend to host higher-stretch SNe Ia than passive galaxies (e.g., Hamuy et al. 2000; Neill et al. 2009; Hicken et al. 2009). For example, Sullivan et al. (2006b) find a formal difference between the stretches of SNe Ia hosted by passive and star-forming galaxies at $z > 0.1$, with stretch medians of ~ 0.93 and ~ 0.98, respectively. Our sample has stretch medians of 0.95 (1.0) for the 43 (47) SNe Ia hosted by passive (star-forming) galaxies, which is a stretch difference of the same sense and similar magnitude to those seen by previous studies. However, a number of statistical tests (χ^2, Kolmogorov-Smirnov, Student) all indicate that, in the case of our sample, these differences are not significant. Whereas the apparent statistical accuracy of our stretch measurement, ± 0.03, is similar to that of Sullivan et al. (2006b), ± 0.01–0.02, our measurements might suffer from systematic or larger statistical uncertainties currently unaccounted for.

When using the figure of merit χ_λ^2 introduced in Section 3.1, we optimize our detection and classification method towards the discovery of SNe Ia, and recover only two of the ten SNe IIP in Table 4, due to the relatively smaller wavelength ranges covered by the SNID SN IIP templates. This, together with the overall small size of the SN IIP sample, precludes deriving a SN IIP rate in the context of this work.

5   SUPERNOVA RATE ANALYSIS

5.1   Visibility time

In order to measure SN Ia rates, we calculate a visibility time for each galaxy in our sample. This is the period of time during which we could have detected a SN Ia at that galaxy's

Table 4. SNe discovered in SDSS DR7

SDSS ID	Date	α	δ	z	Age$_1$	Age$_2$	s	r'_{SN}	r'_H	χ^2_{gal}	χ^2_{SN}	Type
(1)	(2)	(3)	(4)	(5)	(6)	(7)	(8)	(9)	(10)	(11)	(12)	(13)
0271-51883-171	05/12/00	154.5020	−0.0328	0.065	27	42	0.91	19.54	18.11	2.4	1.2	Ia
0291-51928-076	19/01/01	191.8892	0.0992	0.086	28	21	1.06	20.03	17.87	1.7	1.0	Ia
0313-51673-154	09/05/00	231.8958	−0.0595	0.044	33	38	1.11	19.85	17.43	1.6	1.1	Ia
0328-52282-570	08/01/02	175.9218	−1.4770	0.125	27	30	0.84	19.94	17.99	1.5	1.1	Ia
0358-51818-181	01/10/00	263.1189	56.0737	0.123	21	30	1.05	20.19	18.21	1.7	1.1	Ia
0394-51812-554	25/09/00	14.0069	0.4353	0.146	−5	−5	1.12	20.03	18.08	1.3	1.0	Ia
0418-51884-144	06/12/00	9.8403	14.4699	0.017	12	16	1.04	19.46	17.36	2.1	1.1	Ia
0424-51893-355	15/12/00	19.6493	14.6835	0.054	7	7	0.94	17.97	16.98	7.6	1.1	Ia
0438-51884-166	06/12/00	121.0888	46.7870	0.187	16	12	0.88	21.30	18.16	1.1	1.0	Ia
0438-51884-462	06/12/00	120.8026	47.6138	0.117	2	−5	0.91	19.54	18.06	2.2	1.0	Ia
0452-51911-319	02/01/01	140.6214	57.9081	0.063	9	10	0.83	19.43	17.93	1.8	1.1	Ia
0480-51989-024	21/03/01	147.9711	1.1016	0.063	2	−8	1.00	18.77	17.77	4.4	1.5	Ia
0498-51984-102	16/03/01	212.7430	64.8475	0.141	20	18	0.99	20.43	18.09	1.2	0.9	Ia
0500-51994-100	26/03/01	149.8156	0.9673	0.088	11	9	0.98	19.64	18.43	1.8	1.0	Ia
0578-52339-314	06/03/02	159.7062	4.0156	0.129	6	3	1.04	19.54	17.87	1.8	1.2	Ia
0604-52079-209	19/06/01	204.9366	62.3936	0.136	2	−5	0.95	20.11	18.38	1.2	1.0	Ia
0606-52365-412	01/04/02	213.3167	62.0323	0.142	6	−2	0.88	20.15	17.45	1.4	1.2	Ia
0622-52054-011	25/05/01	244.3058	48.4744	0.104	16	17	1.07	19.88	18.21	1.7	1.3	Ia
0738-52521-360	04/09/02	336.7925	13.6661	0.150	27	22	1.04	20.19	18.14	1.1	1.0	Ia
0745-52258-092	15/12/01	350.7757	13.6668	0.041	54	68	0.89	20.16	17.40	1.1	0.9	Ia
0762-52232-067	19/11/01	129.7765	43.7123	0.125	31	34	1.06	20.39	18.03	1.0	0.9	Ia
0814-52443-249	18/06/02	243.4005	43.7256	0.112	8	7	0.96	20.01	18.18	1.5	0.9	Ia
0844-52378-462	14/04/02	184.4150	5.3234	0.104	31	36	1.05	20.32	17.85	1.2	1.0	Ia
0905-52643-213	04/01/03	157.4940	53.5018	0.137	42	38	1.02	20.60	18.25	1.0	0.9	Ia
0915-52443-543	18/06/02	211.3174	−1.7113	0.054	29	24	1.03	19.33	17.44	1.5	0.9	Ia
0966-52642-221	03/01/03	172.2523	48.7331	0.074	3	2	0.89	19.46	18.26	1.8	1.1	Ia
1038-52673-135	03/02/03	191.8526	53.7308	0.153	12	11	0.88	20.59	19.08	1.2	1.0	Ia
1059-52618-144	10/12/02	116.8937	27.4465	0.063	33	32	1.04	19.43	17.51	1.9	0.9	Ia
1171-52753-185	24/04/03	244.8403	41.0899	0.038	10	8	0.89	18.00	16.16	3.9	0.9	Ia
1189-52668-239	29/01/03	132.2645	5.8377	0.126	3	4	0.78	20.01	18.07	1.4	1.0	Ia
1205-52670-632	31/01/03	122.8267	26.1661	0.144	12	13	0.97	20.25	17.58	1.3	1.1	Ia
1278-52735-425	06/04/03	189.1061	50.6116	0.106	6	6	0.95	19.51	17.64	1.5	1.0	Ia
1289-52734-413	05/04/03	220.2447	45.1308	0.074	8	8	0.93	19.53	16.57	1.0	0.8	Ia
1298-52964-304	21/11/03	129.7903	7.4088	0.046	32	48	0.96	18.92	17.47	2.0	1.0	Ia
1310-53033-459	29/01/04	173.5529	58.2622	0.122	16	14	1.06	19.56	17.67	1.9	0.9	Ia
1324-53088-169	24/03/04	211.9955	54.3631	0.067	52	52	1.06	19.87	17.60	1.5	1.0	Ia
1337-52767-480	08/05/03	245.0462	38.1115	0.130	2	4	0.84	19.80	18.12	1.5	1.0	Ia
1392-52822-147	02/07/03	240.3856	26.9875	0.050	14	14	0.93	17.84	16.90	6.4	1.1	Ia
1400-53470-234	10/04/05	230.1879	36.8118	0.103	6	3	1.03	18.89	16.58	1.8	0.9	Ia
1400-53470-351	10/04/05	229.2268	37.1240	0.116	−9	−14	1.16	19.66	17.21	1.1	0.9	Ia
1403-53227-456	10/08/04	237.2391	33.9571	0.128	27	33	0.84	20.26	18.39	1.2	1.0	Ia
1445-53062-067	27/02/04	177.1144	42.1320	0.086	3	−3	0.89	19.65	17.41	1.3	0.9	Type
1462-53112-638	17/04/04	202.1417	41.8523	0.028	8	7	0.99	16.52	16.53	13.3	1.1	Ia
1581-53149-470	24/05/04	235.1032	32.8659	0.054	30	40	0.90	18.97	17.69	3.3	1.0	Ia
1598-53033-380	29/01/04	155.7088	11.7030	0.102	2	−1	0.92	19.67	17.99	1.6	1.0	Ia
1645-53172-349	16/06/04	217.2314	35.0823	0.121	21	34	1.14	19.97	16.95	1.3	1.0	Ia
1697-53142-506	17/05/04	199.1256	12.6769	0.151	3	4	1.06	19.92	17.66	1.3	0.9	Ia
1700-53502-302	12/05/05	203.6364	11.1324	0.095	3	1	1.21	19.59	16.96	1.3	1.1	Ia
1710-53504-488	14/05/05	219.0440	12.4451	0.085	27	24	0.90	19.70	18.03	1.2	1.0	Ia
1744-53055-210	20/02/04	149.9506	11.4737	0.060	9	9	0.94	18.37	19.20	6.6	1.1	Ia

(1) – SDSS DR7 plate, MJD, and fiber in which the SN was discovered.
(2) – Date on which the SN was captured, in dd/mm/yy.
(3)–(4) – Right ascensions and declinations (J2000).
(5) – SN host-galaxy redshift.
(6)–(7) – SN age, in days, as measured by SVD and SNID, respectively. SN Ia (IIP) ages have an uncertainty of ±6 (33) days.
(8) – SN stretch, as measured with the SALT2 templates. All stretches have an uncertainty of ±0.03.
(9)–(10) – SN and host-galaxy r'-band magnitudes.
(11)–(12) – Reduced χ^2 value of galaxy and galaxy+transient fits.
(13) – SN type.

Table 4. SNe discovered in SDSS DR7 – *continued*

SDSS ID	Date	α	δ	z	Age$_1$	Age$_2$	s	r'_{SN}	r'_H	χ^2_{gal}	χ^2_{SN}	Type
(1)	(2)	(3)	(4)	(5)	(6)	(7)	(8)	(9)	(10)	(11)	(12)	(13)
1755-53386-309	16/01/05	173.1052	14.6202	0.082	21	21	1.10	19.32	17.13	1.7	0.9	Ia
1758-53084-523	20/03/04	127.3894	8.8682	0.112	2	−3	0.85	19.62	17.75	1.6	1.0	Ia
1782-53383-517	13/01/05	126.1666	54.6689	0.063	55	43	1.02	20.02	17.33	1.5	1.0	Ia
1788-54468-126	03/01/08	145.0818	63.2817	0.120	2	−1	1.00	20.46	18.02	1.2	1.0	Ia
1791-54266-583	15/06/07	194.1119	10.2277	0.107	12	10	1.01	19.31	17.65	2.0	1.2	Ia
1793-53883-040	28/05/06	196.4333	9.5797	0.055	52	50	1.01	19.68	17.03	1.4	0.9	Ia
1801-54156-371	25/02/07	202.8033	7.9573	0.123	12	34	1.00	19.81	17.79	1.4	1.1	Ia
1803-54152-260	21/02/07	205.4068	5.8710	0.060	33	40	0.83	19.80	17.11	1.3	1.0	Ia
1843-53816-491	22/03/06	223.2384	31.0742	0.094	55	50	1.08	20.01	17.73	1.5	1.0	Ia
1944-53385-434	15/01/05	144.4477	28.2876	0.153	−1	−5	0.86	20.10	18.49	1.6	1.0	Ia
1949-53433-080	04/03/05	150.8604	32.1330	0.166	3	−5	1.06	20.23	18.08	1.1	0.9	Ia
1957-53415-232	14/02/05	155.6271	35.6764	0.128	21	17	0.95	20.23	18.00	1.2	0.9	Ia
2019-53430-010	01/03/05	161.1689	30.6343	0.072	2	3	1.04	18.87	18.68	4.8	1.6	Ia
2159-54328-161	16/08/07	230.6900	19.7057	0.109	12	12	0.89	19.70	17.65	1.2	0.9	Ia
2165-53917-406	01/07/06	234.5504	25.0456	0.067	27	35	1.07	19.22	17.69	1.3	0.9	Ia
2173-53874-154	19/05/06	240.4273	20.5769	0.123	2	−1	0.87	20.30	17.80	1.4	1.1	Ia
2199-53556-232	05/07/05	240.3188	17.7678	0.045	13	15	0.94	17.84	16.65	10.9	1.5	Ia
2202-53566-403	15/07/05	246.0988	15.6767	0.084	4	4	0.99	18.54	18.45	8.1	1.2	Ia
2218-53816-295	22/03/06	171.5008	26.0536	0.158	6	9	1.01	20.24	17.96	1.4	1.2	Ia
2222-53799-480	05/03/06	176.1602	29.8899	0.076	12	15	0.90	19.29	18.23	3.3	1.1	Ia
2376-53770-183	04/02/06	158.4883	20.3405	0.087	2	−3	1.02	18.88	16.90	2.0	1.0	Ia
2420-54086-142	17/12/06	123.7092	11.7155	0.088	−3	−1	0.94	20.77	18.05	1.5	1.2	Ia
2429-53799-033	05/03/06	132.1170	14.4232	0.069	38	36	1.03	19.75	17.71	1.5	1.0	Ia
2430-53815-267	21/03/06	132.4331	12.2987	0.050	33	36	1.03	19.47	18.77	2.4	1.1	Ia
2499-54176-550	17/03/07	172.2386	17.2243	0.143	−3	−9	0.90	20.11	18.10	1.3	0.9	Ia
2594-54177-348	18/03/07	158.4080	16.6030	0.052	21	23	1.13	20.69	17.48	1.5	1.1	Ia
2603-54479-486	14/01/08	196.4791	17.8272	0.078	28	26	1.06	20.91	18.56	1.2	0.9	Ia
2609-54476-295	11/01/08	181.4544	18.9829	0.168	3	−5	1.12	19.96	18.08	1.6	1.1	Ia
2614-54481-257	16/01/08	190.8844	18.9626	0.168	8	4	1.00	20.42	18.37	1.2	1.0	Ia
2664-54524-468	28/02/08	200.7558	24.5066	0.073	6	6	0.93	19.11	17.63	2.4	1.2	Ia
2744-54272-561	21/06/07	211.5930	16.4834	0.014	40	45	0.99	17.40	15.23	4.5	0.8	Ia
2747-54233-613	13/05/07	218.8254	15.5351	0.107	12	10	0.87	19.90	17.88	1.6	1.1	Ia
2754-54240-593	20/05/07	234.2158	12.1352	0.094	27	26	0.90	19.90	18.09	1.9	1.1	Ia
2758-54523-082	27/02/08	213.1021	17.0065	0.174	6	6	0.93	20.25	18.28	1.4	1.1	Ia
2768-54265-233	14/06/07	233.2249	13.1177	0.073	27	24	1.10	19.54	17.29	1.3	1.0	Ia
2771-54527-05	02/03/08	212.4780	19.6616	0.077	16	17	1.09	20.21	16.91	1.2	1.0	Ia
2792-54556-210	31/03/08	226.3821	17.9847	0.036	13	15	0.93	17.35	16.58	15.7	1.1	Ia
2886-54498-598	02/02/08	164.2943	9.4009	0.088	6	10	0.96	19.86	18.25	2.0	1.3	Ia
2949-54557-440	01/04/08	249.2445	27.1098	0.140	21	22	0.89	20.45	18.52	1.2	1.0	Ia
2954-54561-572	05/04/08	233.5161	2.2105	0.034	−1	5	0.83	18.82	16.76	1.3	0.8	Ia
0437-51869-328	21/11/00	119.5556	44.0190	0.047	19	0	$\cdots$	20.00	17.48	1.5	1.1	IIP
0864-52320-082	15/02/02	129.9163	35.6542	0.160	4	5	$\cdots$	20.00	18.31	1.2	1.0	IIP
1207-52672-512	02/02/03	126.2081	29.6123	0.040	87	36	$\cdots$	20.23	18.06	1.4	1.1	IIP
1231-52725-553	27/03/03	186.9265	9.9579	0.070	34	49	$\cdots$	20.15	18.41	1.2	1.0	IIP
1406-52876-528	25/08/03	243.2197	30.8496	0.048	34	49	$\cdots$	20.25	18.18	1.3	1.0	IIP
1459-53117-022	22/04/04	198.2796	46.0984	0.030	35	50	$\cdots$	19.88	19.33	2.4	1.7	IIP
1684-53239-484	22/08/04	245.6866	32.6592	0.041	62	36	$\cdots$	19.85	17.01	1.9	1.4	IIP
1755-53386-516	16/01/05	174.8064	15.0377	0.014	63	82	$\cdots$	19.51	18.71	3.2	1.2	IIP
2103-53467-081	07/04/05	180.8496	35.3258	0.028	19	34	$\cdots$	19.22	17.48	1.8	0.9	IIP
2593-54175-334	16/03/07	157.8944	19.0687	0.034	35	113	$\cdots$	19.98	19.68	2.0	1.4	IIP

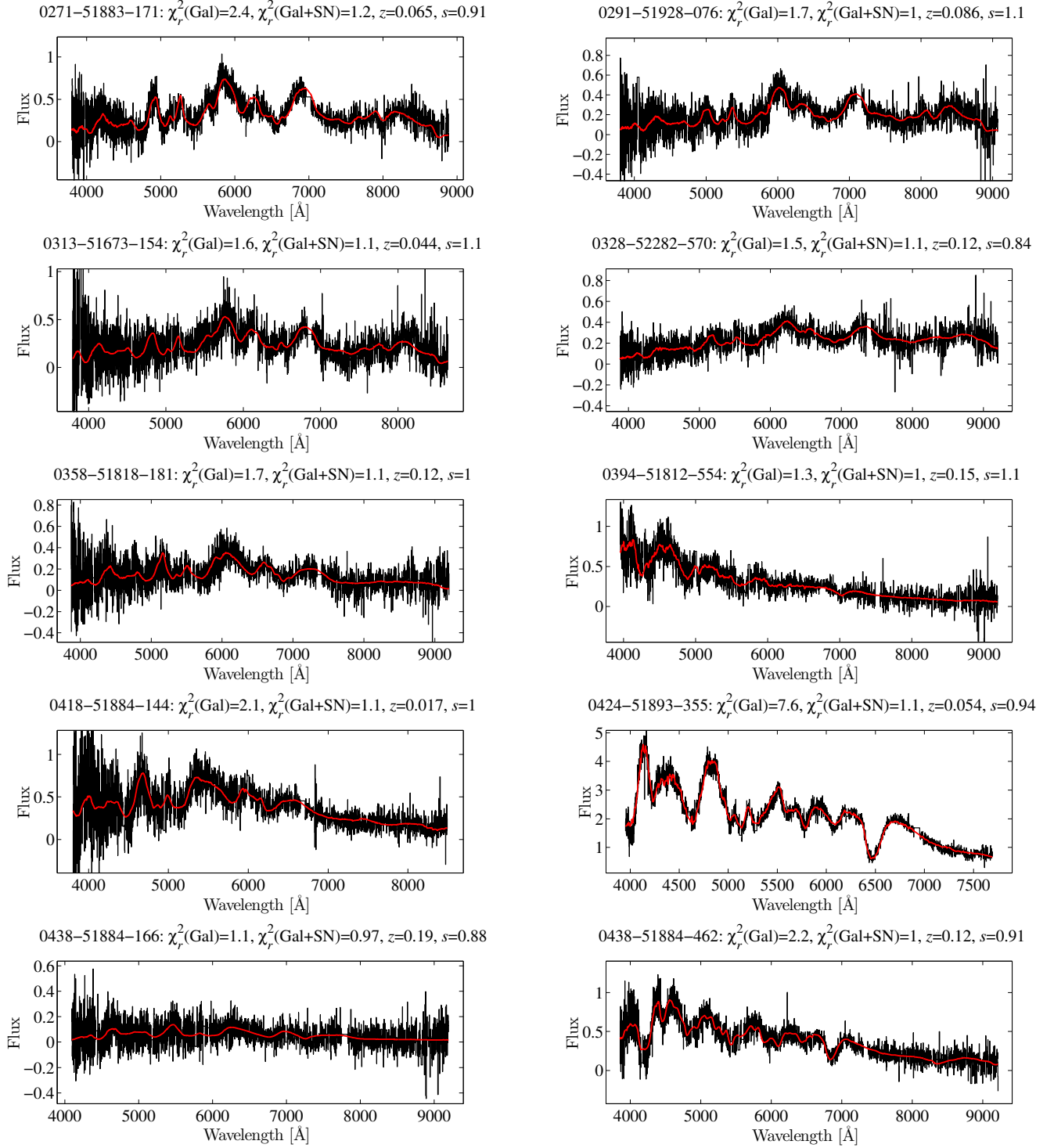(1) – SDSS DR7 plate, MJD, and fiber in which the SN was discovered.
(2) – Date on which the SN was captured, in dd/mm/yy.
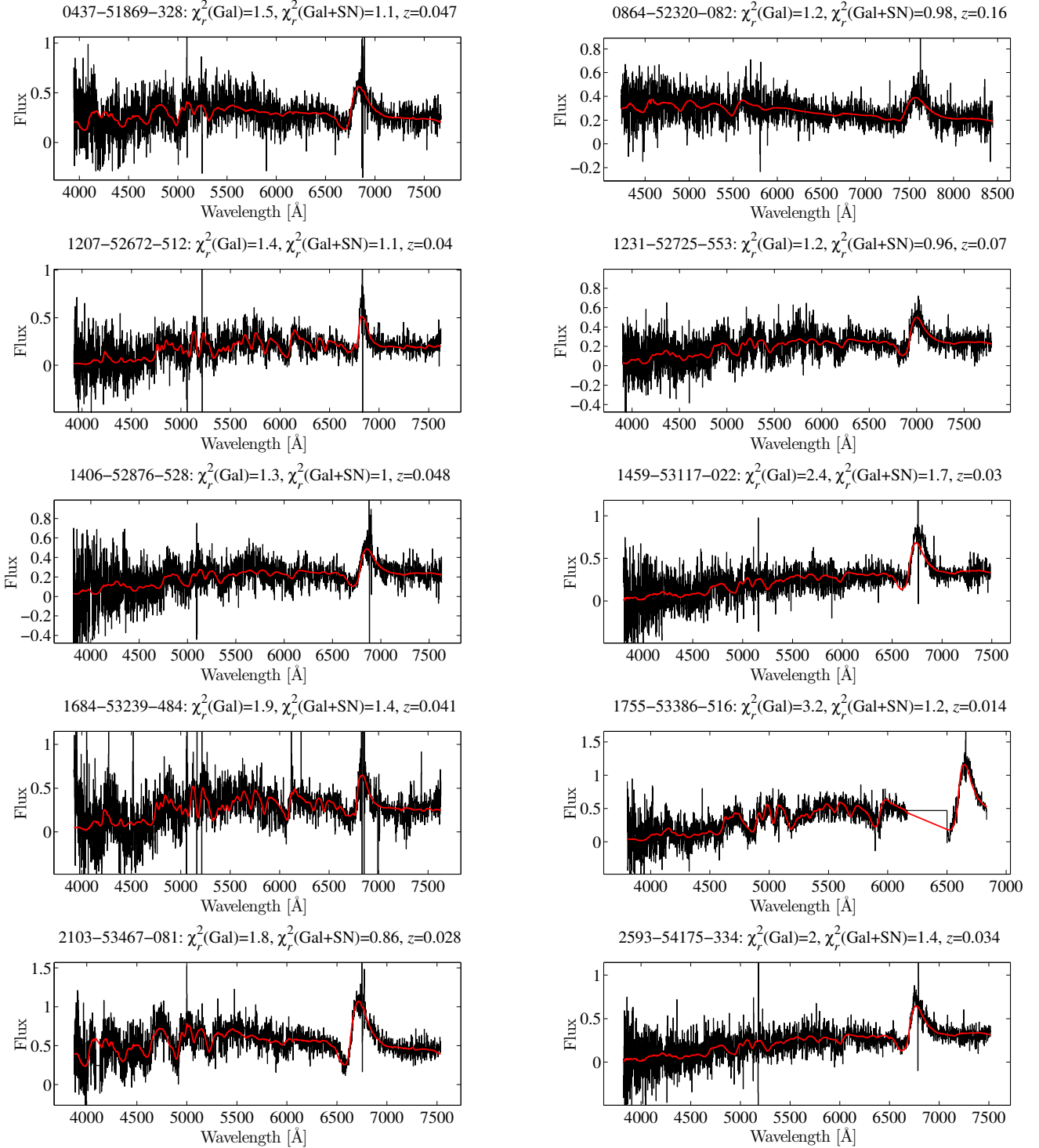(3)–(4) – Right ascensions and declinations (J2000).
(5) – SN host-galaxy redshift.
(6)–(7) – SN age, in days, as measured by SVD and SNID, respectively. SN Ia (IIP) ages have an uncertainty of ± 6 (33) days.
(8) – SN stretch, as measured with the SALT2 templates. All stretches have an uncertainty of ± 0.03.
(9)–(10) – SN and host-galaxy r'-band magnitudes.
(11)–(12) – Reduced χ^2 value of galaxy and galaxy+transient fits.
(13) – SN type.

0271–51883–171: χ^2_r(Gal)=2.4, χ^2_r(Gal+SN)=1.2, z=0.065, s=0.91

0291–51928–076: χ^2_r(Gal)=1.7, χ^2_r(Gal+SN)=1, z=0.086, s=1.1

0313–51673–154: χ^2_r(Gal)=1.6, χ^2_r(Gal+SN)=1.1, z=0.044, s=1.1

0328–52282–570: χ^2_r(Gal)=1.5, χ^2_r(Gal+SN)=1.1, z=0.12, s=0.84

0358–51818–181: χ^2_r(Gal)=1.7, χ^2_r(Gal+SN)=1.1, z=0.12, s=1

0394–51812–554: χ^2_r(Gal)=1.3, χ^2_r(Gal+SN)=1, z=0.15, s=1.1

0418–51884–144: χ^2_r(Gal)=2.1, χ^2_r(Gal+SN)=1.1, z=0.017, s=1

0424–51893–355: χ^2_r(Gal)=7.6, χ^2_r(Gal+SN)=1.1, z=0.054, s=0.94

0438–51884–166: χ^2_r(Gal)=1.1, χ^2_r(Gal+SN)=0.97, z=0.19, s=0.88

0438–51884–462: χ^2_r(Gal)=2.2, χ^2_r(Gal+SN)=1, z=0.12, s=0.91

Figure 8. SNe Ia discovered in SDSS DR7 galaxy spectra. The residual spectrum, obtained by first fitting galaxy eigenspectra and transient templates to the original spectrum, and then subtracting the resulting galaxy model, is shown in black. The best-fitting SN Ia template is overlaid in red. The flux is in units of 10^{-16} erg cm^{-2} s^{-1} Å^{-1}. The title of each panel details the plate, MJD, and fiber in which it was discovered; the reduced χ^2 value obtained when fitting only galaxy eigenspectra to the spectrum, χ^2_r(Gal); the reduced χ^2 obtained from the best-fitting combination of galaxy eigenspectra and transient templates, χ^2_r(Gal+SN); the redshift of the SN-host galaxy, z; and the stretch parameter, s, obtained by using the SALT2 templates. Similar figures for the rest of our SN Ia sample are available in the electronic version of the paper – see Supporting Information.

0437−51869−328: χ^2_r(Gal)=1.5, χ^2_r(Gal+SN)=1.1, z=0.047

0864−52320−082: χ^2_r(Gal)=1.2, χ^2_r(Gal+SN)=0.98, z=0.16

1207−52672−512: χ^2_r(Gal)=1.4, χ^2_r(Gal+SN)=1.1, z=0.04

1231−52725−553: χ^2_r(Gal)=1.2, χ^2_r(Gal+SN)=0.96, z=0.07

1406−52876−528: χ^2_r(Gal)=1.3, χ^2_r(Gal+SN)=1, z=0.048

1459−53117−022: χ^2_r(Gal)=2.4, χ^2_r(Gal+SN)=1.7, z=0.03

1684−53239−484: χ^2_r(Gal)=1.9, χ^2_r(Gal+SN)=1.4, z=0.041

1755−53386−516: χ^2_r(Gal)=3.2, χ^2_r(Gal+SN)=1.2, z=0.014

2103−53467−081: χ^2_r(Gal)=1.8, χ^2_r(Gal+SN)=0.86, z=0.028

2593−54175−334: χ^2_r(Gal)=2, χ^2_r(Gal+SN)=1.4, z=0.034

Figure 9. Same as Fig. 8, for SNe IIP discovered in SDSS DR7 galaxy spectra.

redshift, with specific stretch and host-galaxy extinction values, and the SN Ia detection efficiency curve we measured in Section 3.3. We construct SN Ia light curves using the Hsiao et al. (2007) SN Ia template spectra. Each spectrum is reddened using the Cardelli et al. (1989) extinction law and A_V values drawn from the Neill et al. (2006) extinction model: a one-sided positive Gaussian centred on $A_V = 0$

with a standard deviation of $\sigma = 0.62$. Next, the spectra are redshifted according to the redshift of the galaxy. We apply synthetic photometry to the reddened and redshifted spectra to construct an r'-band light curve. This light curve is then stretched according to Equation 1. Each galaxy in our final sample is assigned a random stretch value from a Gaussian distribution with a standard deviation of $\sigma_s = 0.1$,

and the mean of the Gaussian is selected according to the sSFR of the galaxy: $\mu_s = 1$ ($\mu_s = 0.9$) for star-forming (passive) galaxies (Sullivan et al. 2006a). Following Sullivan et al. (2006a) and Meyers et al. (2012), the stretch values for star-forming (passive) galaxies are restricted to the range $0.6 < s < 1.4$ ($0.6 < s < 1.1$). We use the Yasuda & Fukugita (2010) LF to assign absolute B-band magnitudes at maximum light to each light curve. Each point in the light curve is then multiplied by the appropriate detection efficiency, according to the r'-band magnitude of its host galaxy, as shown in Fig. 3. The visibility time is

$$t_v = \int_{-\infty}^{\infty} \epsilon[m(t)]dt, \qquad (4)$$

where $m(t)$ is the redshifted and reddened template SN Ia light curve in the r' band, and $\epsilon(m)$ is the detection efficiency, as a function of magnitude.

5.2 The rate-mass relation

The mass-normalized SN Ia rate is the number of SNe Ia, $N_{\mathrm{Ia},i}$, in galaxies within a specific mass range i, divided by the sum of the visibility times, $t_{v,j}$, of the n galaxies within that mass range, weighted by their monitored stellar mass, $M_{*,j}$ (i.e., the mass of the galaxy within the spectral aperture, as observed at its present redshift, after mass loss during stellar evolution):

$$R_{\mathrm{Ia},i} = \frac{N_{\mathrm{Ia},i}}{\sum_{j=1}^{n} t_{v,j} M_{*,j}}. \qquad (5)$$

For the total stellar mass of the galaxies in our sample (used only for the purpose of binning the galaxies into various total-mass ranges), we use the VESPA values from T09, with the 0.55 correction, and with the original T09 aperture correction. As in other such studies, we present our rates in units of SNuM (10^{-12} $M_\odot{}^{-1}$ yr^{-1}). We measure the mass-normalized SN Ia rates in four total mass bins, where the limits of the bins are chosen so that each bin contains approximately the same number of SNe Ia. We measure the rates of all galaxies, and specifically of star-forming and passive galaxies, distinguished according to their sSFR, using the previously defined borders. Over the redshift range of our SN Ia sample, $0.014 < z < 0.19$, we do not find a dependence of the rate on redshift, whether for all galaxies or for galaxies separated by sSFR. We therefore analyse together all redshifts in our sample. The cited uncertainties of the rates are the Poisson uncertainties on the number of SNe Ia in each mass bin. These rates are summarized in Table 5.

The mass-normalized SN Ia rate, averaged over all masses and redshifts in our sample, is $R_{\mathrm{Ia,M}} = 0.10 \pm 0.01$ SNuM. For passive galaxies alone, the mass-normalized SN Ia rate is $R_{\mathrm{Ia,M}} = 0.082^{+0.015}_{-0.012}$ SNuM. This last value is consistent with the values obtained by the two other main galaxy-targeted surveys, $0.044^{+0.016}_{-0.014}$ SNuM for E/S0 galaxies (Mannucci et al. 2005), and $0.125^{+0.026}_{-0.022}(0.028)$ [$0.104^{+0.016}_{-0.014}(0.024)$] SNuM for elliptical (S0) galaxies (L11), where the uncertainties are statistical and systematic, respectively.

Fig. 10 shows the SN Ia rate per unit mass, as a function
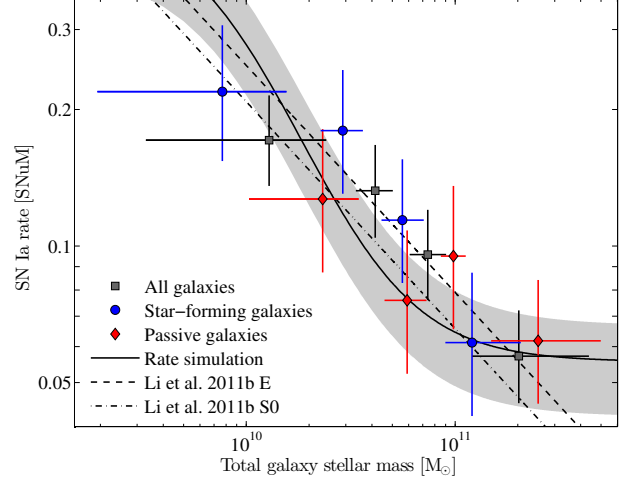
Figure 10. SN Ia rates per unit stellar mass, as a function of total galaxy stellar mass. The mass-normalized SN Ia rates for all galaxies in each mass bin are shown as black squares, while the rates for star-forming (passive) galaxies are shown as blue circles (red diamonds). Vertical error bars are based on the Poisson uncertainty on the number of SNe Ia in the specific mass bin, and the horizontal error bars denote the range within which 68 per cent of the galaxies fall within the mass bin. The solid curve shows the best-fitting SN Ia rate as a function of stellar mass, as derived from a combination of a t^{-1} DTD and the Gallazzi et al. (2005) relation between mass and galaxy age. The shaded area is the confidence region resulting from the 68 per cent statistical uncertainty of the DTD amplitude Ψ_1. The dashed (dot-dashed) curves are the L11 power-law fits to their mass-normalized SN Ia rates in local elliptical (S0) galaxies.

of galaxy mass, for all galaxies in our sample, and separately for passive and star-forming galaxies. The mass-normalized SN Ia rates decrease with increasing galaxy mass. We thus confirm, with the present sample at $z \sim 0.1$, the similar dependence found by L11 for SNe Ia discovered in the local LOSS sample.

Kistler et al. (2011) have recently pointed out that the rate-mass relation found by L11 can be explained by the fact that massive galaxies formed earlier in the cosmic history, combined with a $\sim t^{-1}$ DTD. We repeat here the Kistler et al. (2011) calculation, with some small differences. The mass-normalized SN Ia rate of galaxy i at cosmic time t can be expressed as the convolution of the SFH, $S(t)$, and a DTD, $\Psi(t)$, divided by the total stellar mass of the galaxy, $M_{*,i}$, after mass loss due to stellar evolution:

$$R_{\mathrm{Ia},i}(t) = \frac{1}{M_{*,i}} \int_0^t S(t')\Psi(t-t')dt'. \qquad (6)$$

Following Kistler et al. (2011), we use the Gallazzi et al. (2005) relation between the stellar mass of a galaxy and its age to derive ages for a random selection of 10,000 galaxies with redshifts drawn from the redshift distribution of the SDSS DR7 sample. For each galaxy, we draw a galaxy age from a Gaussian distribution centred on the median values in table 2 from Gallazzi et al. (2005), with the 16/84 per cent values acting as the distribution's lower and upper standard deviations. Following Gallazzi et al. (2005), we use an exponential SFH of the form $e^{-\alpha t}$, with indices α drawn from a

Table 5. Mass-normalized SN Ia rates

mass range [10^{10} M$_\odot$]	median[a] [10^{10} M$_\odot$]	SNe Ia	SN Ia rate[b] [SNuM]
All galaxies			
$0 < M_* < 3$	$1.3^{+1.1}_{-1.0}$	23	$0.171^{+0.044}_{-0.035}$
$3 \leqslant M_* < 5.5$	$4.1^{+0.9}_{-0.8}$	22	$0.132^{+0.035}_{-0.028}$
$5.5 \leqslant M_* < 10$	$7.4^{+1.7}_{-1.3}$	23	$0.096^{+0.024}_{-0.020}$
$M_* \geqslant 10$	20^{+24}_{-8}	22	$0.057^{+0.015}_{-0.012}$
All masses	6^{+16}_{-5}	90	0.10 ± 0.01
Star-forming galaxies			
$0 < M_* < 2$	$0.8^{+0.8}_{-0.6}$	11	$0.22^{+0.09}_{-0.06}$
$2 \leqslant M_* < 4$	$2.9^{+0.7}_{-0.6}$	13	$0.18^{+0.06}_{-0.05}$
$4 \leqslant M_* < 8$	$5.6^{+1.5}_{-1.1}$	13	$0.11^{+0.04}_{-0.03}$
$M_* \geqslant 8$	12^{+9}_{-3}	10	$0.061^{+0.026}_{-0.019}$
All masses	3^{+6}_{-2}	47	$0.118^{+0.020}_{-0.017}$
Passive galaxies			
$0 < M_* < 4$	$2.3^{+1.1}_{-1.3}$	10	$0.13^{+0.05}_{-0.04}$
$4 \leqslant M_* < 8$	$5.9^{+1.4}_{-1.3}$	10	$0.076^{+0.032}_{-0.024}$
$8 \leqslant M_* < 12$	$9.8^{+1.4}_{-1.3}$	10	$0.10^{+0.02}_{-0.03}$
$M_* \geqslant 12$	25^{+25}_{-10}	13	$0.062^{+0.022}_{-0.017}$
All masses	11^{+22}_{-7}	43	$0.082^{+0.015}_{-0.012}$

[a] Uncertainties represent the mass region occupied by 68 per cent of the galaxies in that bin.
[b] Rate uncertainties are Poisson uncertainties on the number of SNe Ia in each mass bin.

flat distribution between 0 and 1. The SFH is scaled to produce the galaxy's formed mass, M_f, over the period of time between a galaxy's formation time, t_g, and t. We assume a power-law DTD with index -1, with the amplitude Ψ_1 at $t = 1$ Gyr left as a free parameter. Equation 6 thus becomes:

$$R_{\mathrm{Ia},i}(t) = \frac{M_f}{M_*} \Psi_1 \int_0^t e^{-\alpha t'} (t - t')^{-1} dt'. \qquad (7)$$

As our measurements cover mainly old galaxies in the mass range $\sim 10^9$–10^{12} M$_\odot$, we set $M_f/M_* = 2.3$ (Bruzual & Charlot 2003). The best-fitting DTD amplitude, with a reduced $\chi_r^2 = 1.5$, is $\Psi_1 = 0.070 \pm 0.016 \times 10^{-12}$ M$_\odot^{-1}$ yr^{-1}, where the uncertainty of Ψ_1 is the 68 per cent confidence region, defined as the range of Ψ_1 values within $\Delta\chi^2 = \pm 1$ of the minimal χ^2 value. The form of the mass-normalized SN Ia rate as a function of mass is similar to the one obtained by Kistler et al. (2011), though with a shallower decline at the high-mass end. Fig. 10 shows the result of this simulation.

Integrating the DTD with the best-fitting value for Ψ_1 over a Hubble time yields a number of SNe Ia per formed stellar mass of $N/M_* = 0.4 \pm 0.1 \times 10^{-3}$ SNe M$_\odot^{-1}$. This value is lower than those obtained by M11 and M12, but consistent with the values obtained by Graur et al. (2011) and P12.

5.3   The Type Ia supernova volumetric rate

We can convert the mass-normalized SN Ia rate, averaged over all masses and redshifts in our sample, to a volumetric rate, by multiplying it by the total cosmic mass density, as inferred from the galaxy stellar mass function (GSMF) measured at $z < 0.06$ by Baldry et al. (2012). However, as the SDSS was a galaxy-targeted survey, we must account for its particular distribution of galaxy mass, M, shown in Fig. 1,

weighted by the rate-mass relation we have found for these galaxies. We do this by multiplying our mass-normalized rate by the ratio of the integrated cosmic GSMF, $B(M)$, to the SDSS DR7 galaxy-mass distribution, $D(M)$ (which is normalized so that $\int D(M)MdM = 1$), where both mass functions are weighted by the rate-mass relation $R(M)$ described in Section 5.2:

$$R_{\mathrm{Ia,V}} = R_{\mathrm{Ia,M}} \frac{\int B(M)R(M)MdM}{\int D(M)R(M)MdM}. \qquad (8)$$

The volumetric SN Ia rate, at a median redshift of $z = 0.11$, is $R_{\mathrm{Ia,V}} = 0.25 \pm 0.03 \times 10^{-4}$ SNe yr^{-1} Mpc^{-3}. The uncertainty in the rate derives from the Poisson uncertainty from the size of the SN Ia sample, along with a systematic uncertainty of -1 SN Ia, as derived from the purity of our discovery and classification method, as detailed in Section 3.3. Varying the GSMF according to the uncertainties reported in table 1 of Baldry et al. (2012) adds a statistical uncertainty an order of magnitude smaller than the Poisson uncertainty, and is thus negligible. With an uncertainty of 12 per cent, this is the most precise rate measurement at this redshift. The uncertainty, however, does not include the systematic uncertainties in the mass estimates of the individual galaxies by T09, an uncertainty that is difficult to estimate. Our volumetric SN Ia rate measurement, along with measurements from other SN surveys in this redshift range, are shown in the upper panel of Fig. 11. Our volumetric rate is in excellent agreement with most previous measurements (e.g., M03; Dilday et al. 2010), but is more precise. Furthermore, our rate merges smoothly with the extrapolation to low redshift of the rates measured by P12 (whose own low-z measurement has large errors). This is shown in the lower panel of Fig. 11. Our low-z rate measurement, together with the P12 measurements, thus provides now a precise picture of the SN Ia rate evolution from $z = 0$ to 1. Following Graur et al. (2011) and P12, we convolve a power-law DTD with different cosmic SFHs (see Graur et al. 2011, section 8) and fit our volumetric SN Ia rate, together with those of P12 and Graur et al. (2011, see Fig. 11). We find a best-fitting index of $-1 \pm 0.1 \pm 0.16$, where the uncertainties are statistical and systematic, respectively, and the systematic uncertainty derives from the different SFHs used in the fit. Taking into account the statistical and systematic uncertainties derived from the cosmic SFHs used in Graur et al. (2011), N/M_* lies in the range $N/M_* = (0.4–1.2) \times 10^{-3}$ SNe M$_\odot^{-1}$.

Our rate calculation is improved compared to the SN Ia rates derived by the two previous studies that have searched for SNe in SDSS spectra. M03 estimated the B-band-luminosity-weighted SN Ia rate at $z \approx 0.1$ using the average galaxy luminosity value of their sample, and a fixed visibility time estimated at $t_v = 20$ days. They obtained 0.4 ± 0.2 h^2 SNuB (10^{-12} L$_{\mathrm{B},\odot}^{-1}$ yr^{-1}), where $h = 100$ km s^{-1} Mpc^{-1}. Horesh et al. (2008) converted this rate into a volumetric rate of $0.24 \pm 0.12 \times 10^{-4}$ SNe yr^{-1} Mpc^{-3} using the redshift-dependent Botticella et al. (2008) luminosity density function, but without taking into account the then-unknown rate-mass relation, which weights the particular luminosity distribution of the galaxies in the SDSS DR1 sample. Similarly, K11 obtained their volumetric rate, $0.569^{+0.098,+0.058}_{-0.085,-0.047} \times 10^{-4}$ SNe yr^{-1} Mpc^{-3} (the errors are statistical and systematic, respectively) by converting their B-band-luminosity-weighted rate of $0.472^{+0.081,+0.048}_{-0.071,-0.039}$ SNuB

using the same redshift-dependent luminosity density function, again without accounting for the effect of the rate-mass relation. Finally, neither M03 or K11 made use of the detailed spectral information available for every galaxy in the sample, which can give the stellar masses of the galaxies (and which we have used for calculating rates, above) and the SFHs of the galaxies (which we use for recovering the DTD, below).

5.4 The Type Ia supernova delay-time distribution

The VESPA SFHs that are available for each of the individual galaxies that were effectively 'monitored' by our SN survey permit applying to the data the M11 algorithm for recovering the DTD. In this approach, briefly, Eq. 6 is approximated by a discretised form,

$$N_i = \sum_j m_{ij} \Psi_j \Delta t_i, \qquad (9)$$

where N_i is the expectation value of the SNe Ia in the ith galaxy, m_{ij} is the stellar mass formed in the galaxy over the jth time interval, Ψ is a binned version of the DTD, and Δt_i is the visibility time of the ith galaxy. The sum is over the three VESPA time bins: < 0.42 Gyr ('prompt'), 0.42–2.4 Gyr ('intermediate'), and > 2.4 Gyr ('delayed'). The values of Ψ_j are treated as free parameters that are scanned so as to best match N_i to the Poisson statistics of the observed sample, which has zero SNe in most of the monitored galaxies, and one SN in a small fraction of the galaxies. M11, analysing the LOSS sample of L11, detected significant prompt and delayed components to the DTD. Applying the method to a sample of SNe Ia from the SDSS-II survey (Dilday et al. 2010; Sako et al. 2011), M12 obtained 4σ detections of all three DTD components.

For the current SN Ia sample and the VESPA-derived SFHs for our galaxies, we obtain a strong detection of a delayed component in the age bin > 2.4 Gyr, of $4.5 \pm 0.6 \times 10^{-14}$ SNe $M_\odot^{-1}$ yr^{-1}. Our recovered delayed component of the SN Ia DTD, along with measurements from other SN surveys, are shown in the Fig. 12. Our delayed component measurement is 2–3 times higher than the corresponding value in M12, but similar to the value obtained by M11. It is possible that this result is affected systematically by the 'flux flow' problem we have identified in galaxies that hosted SNe. Some of the blue light of a host galaxy, light from a young or intermediate-age stellar population, is removed from the galaxy spectrum by the SN Ia template subtraction. As a result, some of the DTD signal could 'drift' from the prompt and intermediate bins to the delayed bin.

We do not detect prompt and intermediate components to the DTD. In retrospect, this is unsurprising, since our galaxy sample is dominate by old and massive galaxies, with little ongoing star formation. 90 SNe Ia were hosted by the 707,792 galaxies in our sample. Of these, only 5,394 galaxies have log(sSFR/yr^{-1}) > -9.5, none of which hosted a SN Ia. The SDSS-II sample used in M12, on the other hand, is composed of 66,400 galaxies, which hosted a total of 132 SNe Ia. 3,867 galaxies had log(sSFR/yr^{-1}) > -9.5, seven of which hosted a SN. Comparing between the two samples, we would have expected $(66{,}400/707{,}792) \times (5{,}394/3{,}867) \times (90/132) \times 7 = 0.6$ SNe Ia in the highly-star-forming galaxies in our
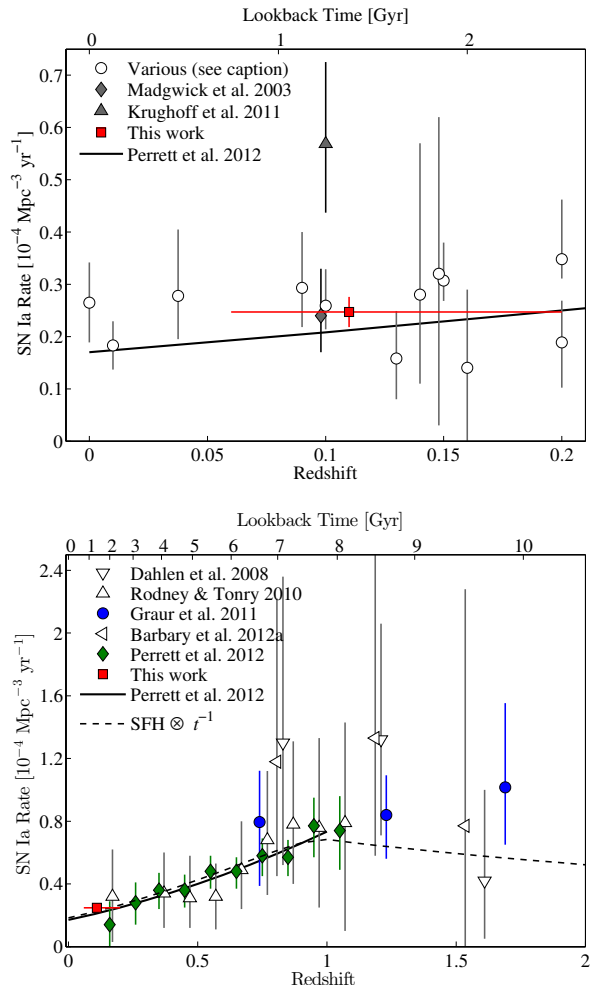
Figure 11. SN Ia volumetric rate at $z = 0.11$ (red square) compared to rates from the literature. Upper panel: circles denote results by Cappellaro, Evans, & Turatto (1999); Hardin et al. (2000); Blanc et al. (2004); Horesh et al. (2008); Dilday et al. (2010); Rodney & Tonry (2010); L11; and P12. The M03 measurement, based on a spectroscopic SN search in SDSS DR1, is the black diamond, and the K11 measurement, based on SDSS DR5, is the black upright triangle. The curve is the fit by P12 to their measured SN Ia rates between $z = 0.1$ and 1. All vertical error bars include statistical and systematic uncertainties. The horizontal error bar indicates the range that encompasses 68 per cent of the SDSS DR7 galaxies around the median redshift of $z = 0.11$. Lower panel: our low-z SN Ia rate (red square) compared to recent high-z rates: Dahlen, Strolger, & Riess (2008) (downturned triangles), Rodney & Tonry (2010) (upturned triangles), Graur et al. (2011) (blue circles), Barbary et al. (2012a) (leftfacing triangles), and P12 (green diamonds). The solid curve is the same as above, and the dashed curve is the best-fitting SN Ia rate evolution derived from convolving the Yüksel et al. (2008) cosmic SFH with a power-law DTD and fitting our volumetric rate measurement, together with those of P12 and Graur et al. (2011). The most precise measurements in each redshift range are marked with filled symbols.
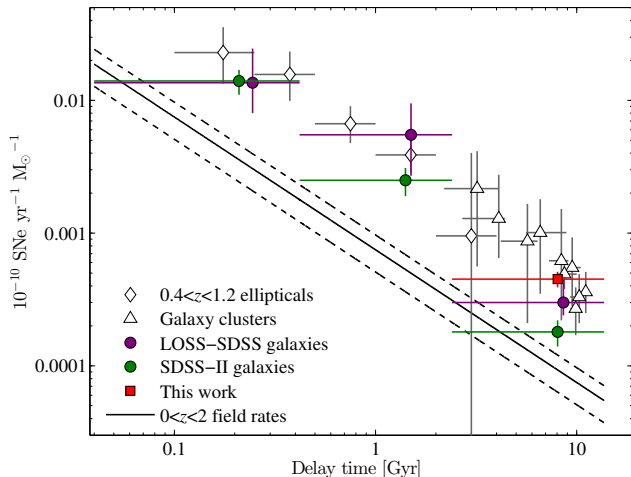
Figure 12. Recovered 'delayed' SN Ia DTD component (red square) compared to previous measurements from the literature: Totani et al. (2008) DTD measurements from SNe Ia discovered in $0.4 < z < 1.2$ elliptical galaxies (diamonds); galaxy cluster surveys (triangles; Maoz et al. 2010 and references therein; Sand et al. 2012); and the 'prompt', 'intermediate', and 'delayed' components recovered with the M11 method (purple; M11 and green; M12) circles. The solid curve is a t^{-1} DTD that, when convolved with the Yüksel et al. (2008) cosmic SFH, provides the best fit to our volumetric rate, together with those of P12 and Graur et al. (2011, see Fig. 11). The dashed curves are the systematic uncertainty on the amplitude of the DTD, derived from using different cosmic SFHs.

sample, which is consistent with our having found none. With no detected SNe Ia in young galaxies, our method is unable to reconstruct the short- and intermediate-delay DTD components.

For the time-integrated number of SNe Ia per formed stellar mass, the M11 recovery method gives $N/M_* = 0.5 \pm 0.2 \times 10^{-3}$ SNe $M_\odot^{-1}$. This is several times lower than the values found by M11 and M12, which is not surprising, given that our survey misses the dominant prompt- and intermediate-delay SN Ia population.

6   SUMMARY AND CONCLUSIONS

We have surveyed the $\sim 700,000$ galaxy spectra in SDSS DR7 that have VESPA-derived SFHs, and discovered and classified 90 SNe Ia and 10 SNe IIP. The purity of our detection and classification routine is such that there is, at most, a 1 per cent systematic uncertainty in the classification of the SNe Ia. Using our SN Ia sample, together with the VESPA-derived stellar masses of the galaxies we survey, we measure the mass-normalized SN Ia rates at a median redshift of $z = 0.11$ and find that they follow the so-called 'rate-size', or rate-mass, relation, which was previously observed in the local Universe by L11. We confirm that more massive galaxies have lower SN Ia rates per unit stellar mass, and that, for galaxies of a given total mass, the mass-normalized SN Ia rate is weakly dependent on the galaxy's sSFR. Following Kistler et al. (2011), we also confirm that this rate-mass relation is essentially a coincidental 'conspiracy'. On the one

hand, less massive galaxies tend to form later in the history of the Universe ('downsizing'). On the other hand, numerous recent SN Ia rate studies point to a DTD that peaks at short delays and decreases monotonically with time (Maoz et al. 2010; Maoz & Badenes 2010; Graur et al. 2011; M11; M12; Barbary et al. 2012b; Badenes & Maoz 2012; P12). The rate-mass relation results from the fact that, for more massive galaxies, we are probing further down along the delayed tail of the DTD. Our mass-normalized SN Ia rates cover a mass range of $\sim 10^9$–10^{12} $M_\odot$. In the future, it would be interesting to extend the mass-normalized SN Ia rates to both lower and higher galaxy masses, where our (albeit simplified) calculation predicts that the rate per unit mass will plateau.

We have also derived a mass-normalized SN Ia rate, averaged over all masses and redshifts in our galaxy sample, 0.10 ± 0.01 SNuM, and a volumetric rate, $R_{\rm Ia,V}(z = 0.11) = 0.25 \pm 0.03 \times 10^{-4}$ SNe yr^{-1} Mpc^{-3}. The latter is the most precise rate measurement at this redshift, and is consistent both with previous measurements from other surveys, and with the low-redshift extrapolation of the power-law fit to the SN Ia rate measurements of P12.

As the SDSS DR7 galaxy sample is composed mainly of massive, old galaxies, applying the direct DTD recovery method of M11 yields only a 'delayed' component of $4.5 \pm 0.6 \times 10^{-14}$ SNe $M_\odot^{-1}$ yr^{-1} in the delay-time range > 2.4 Gyr. This value is 2–3 times higher than the corresponding value in M12, but similar to the value obtained by M11. The differences may be due to a systematic flux flow problem that exists in our SN discovery process. We find that the time-integrated number of SNe Ia per unit formed stellar mass derived from a power-law DTD with index -1 and scaled to yield the above value, is $N/M_* = 0.5 \pm 0.2 \times 10^{-3}$ SNe $M_\odot^{-1}$, consistent with the values obtained by Graur et al. (2011) and P12, but lower than those obtained by M11 and M12. However, the value we find here is likely underestimated due to the fact that our survey monitors, as noted, a predominantly old and massive galaxy population, and therefore samples only a fraction of the SNe Ia in the DTD.

In terms of the progenitor question, our results lend further support to previous indications for a power-law DTD with an index ~ -1. This support comes through the rate-mass relation that we measure (which is naturally explained with such a DTD), through the delayed DTD component we recover directly (this component is part of the above DTD), and through the precise volumetric rate we find (which merges smoothly with rates at higher redshifts and, compared to the cosmic SFH, implies such a DTD). It remains to be seen whether theoretical SD models may produce such a DTD, or whether this result indicates that many, most, or all SNe Ia arise through the DD channel. Further studies, using both SN Ia rates and other relevant techniques, will shed light on this issue.

While large photometric SN surveys, such as the SDSS SN Survey (Dilday et al. 2010; Sako et al. 2011), Supernova Legacy Survey (Neill et al. 2006; P12), and the ongoing Palomar Transient Factory (Rau et al. 2009) have generated large samples of SNe of all types, they require costly spectroscopic followup in order to robustly classify their candidates. Massive spectroscopic surveys, such as previous data releases of the SDSS or the ongoing SDSS-III (Eisenstein et al. 2011),

provide an ideal platform for our code, with which one can assemble large transient samples at no extra cost. The detection and classification method introduced here can be improved upon by, e.g., optimizing it for other types of SNe and by replacing the template library with bases of SN eigenspectra, similar to the SALT2 templates. Furthermore, we will search for ways to discover new types of transients that cannot be fitted with current spectral templates. Finally, although the current work has been an archival search, there is no obstacle to discovering SNe in spectra in real time, while the SNe can still be followed up. We are currently applying such an approach to spectra from the SDSS-III Baryon Oscillation Spectroscopic Survey (Dawson et al. 2012).

REFERENCES

Abazajian K. N. et al., 2009, ApJS, 182, 543
Astier P. et al., 2006, A&A, 447, 31
Badenes C., Maoz D., 2012, ApJ, 749, L11
Baldry I. K. et al., 2012, MNRAS, 421, 621
Barbary K. et al., 2012a, ApJ, 745, 31
—, 2012b, ApJ, 745, 32
Blanc G. et al., 2004, A&A, 423, 881
Blondin S., Tonry J. L., 2007, ApJ, 666, 1024
Bloom J. S. et al., 2012, ApJ, 744, L17
Botticella M. T. et al., 2008, A&A, 479, 49

Brandt T. D., Tojeiro R., Aubourg É., Heavens A., Jimenez R., Strauss M. A., 2010, AJ, 140, 804
Brown P. J. et al., 2012, ApJ, 753, 22
Bruzual G., Charlot S., 2003, MNRAS, 344, 1000
Cappellaro E., Evans R., Turatto M., 1999, A&A, 351, 459
Cardelli J. A., Clayton G. C., Mathis J. S., 1989, ApJ, 345, 245
Chabrier G., 2003, PASP, 115, 763
Chomiuk L. et al., 2012, ApJ, 750, 164
Dahlen T., Strolger L., Riess A. G., 2008, ApJ, 681, 462
Dawson K. S. et al., 2012, preprint (arXiv:1208.0022)
Di Stefano R., Voss R., Claeys J. S. W., 2011, ApJ, 738, L1
Di Stefano R., Kilic M., 2012, preprint (arXiv:1205.3168D)
Dilday B. et al., 2010, ApJ, 713, 1026
Dilday B. et al., 2012, preprint (arXiv:1207.1306D)
Eisenstein D. J. et al., 2011, AJ, 142, 72
Gallazzi A., Charlot S., Brinchmann J., White S. D. M., Tremonti C. A., 2005, MNRAS, 362, 41
Graur O. et al., 2011, MNRAS, 417, 916
Guy J. et al., 2007, A&A, 466, 11
Hachisu I., Kato M., Nomoto K., 2012, ApJ, 756, L4
Hamuy M., Trager S. C., Pinto P. A., Phillips M. M., Schommer R. A., Ivanov V., Suntzeff N. B., 2000, AJ, 120, 1479
Hamuy M. et al., 2003, Nature, 424, 651
Hardin D. et al., 2000, A&A, 362, 419
Hicken M., Garnavich P. M., Prieto J. L., Blondin S., DePoy D. L., Kirshner R. P., Parrent J., 2007, ApJ, 669, L17
Hicken M., Wood-Vasey W. M., Blondin S., Challis P., Jha S., Kelly P. L., Rest A., Kirshner R. P., 2009, ApJ, 700, 1097
Horesh A., Poznanski D., Ofek E. O., Maoz D., 2008, MNRAS, 389, 1871
Horesh A. et al., 2012, ApJ, 746, 21
Howell D. A. et al., 2006, Nature, 443, 308
Howell D. A., 2011, Nature Communications, 2
Hsiao E. Y., Conley A., Howell D. A., Sullivan M., Pritchet C. J., Carlberg R. G., Nugent P. E., Phillips M. M., 2007, ApJ, 663, 1187
Iben Jr. I., Tutukov A. V., 1984, ApJS, 54, 335
Kistler M. D., Stanek K. Z., Kochanek C. S., Prieto J. L., Thompson T. A., 2011, preprint (arXiv:1106.3115K)
Krughoff K. S., Connolly A. J., Frieman J., SubbaRao M., Kilper G., Schneider D. P., 2011, ApJ, 731, 42 (K11)
Leaman J., Li W., Chornock R., Filippenko A. V., 2011, MNRAS, 412, 1419
Li W. et al., 2001, PASP, 113, 1178
Li W. et al., 2003, PASP, 115, 453
Li W. et al., 2011a, MNRAS, 412, 1441
Li W., Chornock R., Leaman J., Filippenko A. V., Poznanski D., Wang X., Ganeshalingam M., Mannucci F., 2011b, MNRAS, 412, 1473 (L11)
Li W. et al., 2011c, Nature, 480, 348
Madgwick D. S., Hewett P. C., Mortlock D. J., Wang L., 2003, ApJ, 599, L33 (M03)
Mannucci F., Della Valle M., Panagia N., Cappellaro E., Cresci G., Maiolino R., Petrosian A., Turatto M., 2005, A&A, 433, 807
Mannucci F., Della Valle M., Panagia N., 2006, MNRAS, 370, 773

Maoz D., Badenes C., 2010, MNRAS, 968

Maoz D., Sharon K., Gal-Yam A., 2010, ApJ, 722, 1879

Maoz D., Mannucci F., Li W., Filippenko A. V., Valle M. D., Panagia N., 2011, MNRAS, 412, 1508 (M11)

Maoz D., Mannucci F., 2011, preprint (arXiv:1111.4492M)

Maoz D., Mannucci F., Brandt T. D., 2012, preprint (arXiv:1206.0465M) (M12)

Maraston C., 2005, MNRAS, 362, 799

Meyers J. et al., 2012, ApJ, 750, 1

Neill J. D. et al., 2006, AJ, 132, 1126

Neill J. D., et al., 2009, ApJ, 707, 1449

Nomoto K., Iben Jr. I., 1985, ApJ, 297, 531

Nugent P., Kim A., Perlmutter S., 2002, PASP, 114, 803

Nugent P. E. et al., 2011, Nature, 480, 344

Oke J. B., Gunn J. E., 1983, ApJ, 266, 713

Pakmor R., Kromer M., Röpke F. K., Sim S. A., Ruiter A. J., Hillebrandt W., 2010, Nature, 463, 61

Pakmor R., Hachinger S., Röpke F. K., Hillebrandt W., 2011, A&A, 528, A117

Pakmor R., Kromer M., Taubenberger S., Sim S. A., Röpke F. K., Hillebrandt W., 2012, ApJ, 747, L10

Patat F. et al., 2007, Science, 317, 924

Perlmutter S. et al., 1999, ApJ, 517, 565

Perrett K. et al., 2012, AJ, 144, 59 (P12)

Phillips M. M. et al., 2007, PASP, 119, 360

Prieto J. L. et al., 2007, preprint (arXiv:0706.4088)

Rau A. et al., 2009, PASP, 121, 1334

Rodney S. A., Tonry J. L., 2010, ApJ, 723, 47

Sako M. et al., 2011, ApJ, 738, 162

Sand D. J. et al., 2012, ApJ, 746, 163

Schaefer B. E., Pagnotta A., 2012, Nature, 481, 164

Shappee B. J., Kochanek C. S., Stanek K. Z., 2012, preprint (ArXiv1205.5028S)

Sharon K. et al., 2010, ApJ, 718, 876

Shen K. J., Bildsten L., Kasen D., Quataert E., 2012, ApJ, 748, 35

Simon J. D. et al., 2009, ApJ, 702, 1157

Sternberg A. et al., 2011, Science, 333, 856

Sullivan M. et al., 2006a, AJ, 131, 960

Sullivan M. et al., 2006b, ApJ, 648, 868

Tojeiro R., Heavens A. F., Jimenez R., Panter B., 2007, MNRAS, 381, 1252

Tojeiro R., Wilkins S., Heavens A. F., Panter B., Jimenez R., 2009, ApJS, 185, 1 (T09)

Totani T., Morokuma T., Oda T., Doi M., Yasuda N., 2008, PASJ, 60, 1327

van Kerkwijk M. H., Chang P., Justham S., 2010, ApJ, 722, L157

Vanden Berk D. E. et al., 2001, AJ, 122, 549

Wang B., Han Z., 2012, NewAR, 56, 122

Webbink R. F., 1984, ApJ, 277, 355

Whelan J., Iben Jr. I., 1973, ApJ, 186, 1007

Yasuda N., Fukugita M., 2010, AJ, 139, 39

Yip C. W. et al., 2004a, AJ, 128, 585

Yip C. W. et al., 2004b, AJ, 128, 2603

York D. G. et al., 2000, AJ, 120, 1579

Yüksel H., Kistler M. D., Beacom J. F., Hopkins A. M., 2008, ApJ, 683, L5